



Metaplastic Reinforcement of Long-Term Potentiation in Hippocampal Area CA2 by Cholinergic Receptor Activation

Amrita Benoy,^{1,2}  Mohammad Zaki Bin Ibrahim,^{1,2} Thomas Behnisch,³ and  Sreedharan Sajikumar^{1,2,4}

¹Department of Physiology, Yong Loo Lin School of Medicine, National University of Singapore, Singapore, 117597, ²Life Sciences Institute Neurobiology Programme, National University of Singapore, Singapore, 117456, ³Institutes of Brain Science, State Key Laboratory of Medical Neurobiology and MOE Frontiers Center for Brain Science, Fudan University, Shanghai, China, 200032 and ⁴Healthy Longevity Translational Research Programme, Yong Loo Lin School of Medicine, National University of Singapore, Singapore, 117456

Hippocampal CA2, an inconspicuously positioned area between the well-studied CA1 and CA3 subfields, has captured research interest in recent years because of its role in social memory formation. However, the role of cholinergic inputs to the CA2 area for the regulation of synaptic plasticity remains to be fully understood. We show that cholinergic receptor activation with the nonselective cholinergic agonist, carbachol (CCh), triggers a protein synthesis-dependent and NMDAR-independent long-term synaptic depression (CCh-LTD) at entorhinal cortical (EC)-CA2 and Schaffer collateral (SC)-CA2 synapses in the hippocampus of adult male Wistar rats. The activation of muscarinic acetylcholine receptors (mAChRs) is critical for the induction of CCh-LTD with the results suggesting an involvement of M3 and M1 mAChRs in the early facilitation of CCh-LTD, while nicotinic AChR activation plays a role in the late maintenance of CCh-LTD at CA2 synapses. Remarkably, we find that CCh priming lowers the threshold for the subsequent induction of persistent long-term potentiation (LTP) of synaptic transmission at EC-CA2 and the plasticity-resistant SC-CA2 pathways. The effects of such a cholinergic-dependent synaptic depression on subsequent LTP at EC-CA2 and SC-CA2 synapses have not been previously explored. Collectively, the results demonstrate that CA2 synaptic learning rules are regulated in a metaplastic manner, whereby modifications triggered by prior cholinergic stimulation can dictate the outcome of future plasticity events. Moreover, the reinforcement of LTP at EC inputs to CA2 following the priming stimulus coexists with concurrent sustained CCh-LTD at the SC-CA2 pathway and is dynamically scaled by modulation of SC-CA2 synaptic transmission.

Key words: acetylcholine; hippocampal CA2; LTD; LTP; metaplasticity; cholinergic receptors

Significance Statement

The release of the neuromodulator acetylcholine is critically involved in processes of hippocampus-dependent memory formation. Cholinergic afferents originating in the medial septum and diagonal bands of Broca terminating in the hippocampal area CA2 might play an important role in the modulation of area-specific synaptic plasticity. Our findings demonstrate that cholinergic receptor activation induces an LTD of synaptic transmission at entorhinal cortical- and Schaffer collateral-CA2 synapses. This cholinergic activation-mediated LTD displays a bidirectional metaplastic switch to LTP on a future timescale. This suggests that such bidirectional synaptic modifications triggered by the dynamic modulation of tonic cholinergic receptor activation may support the formation of CA2-dependent memories given the increased hippocampal cholinergic tone during active wakefulness observed in exploratory behavior.

Received Nov. 13, 2020; revised Sep. 13, 2021; accepted Sep. 18, 2021.

Author contributions: A.B., T.B., and S.S. designed research; A.B. and M.Z.B.I. performed research; A.B., T.B., and S.S. analyzed data; A.B. wrote the first draft of the paper; A.B. and S.S. wrote the paper; T.B. edited the paper.

This work was supported by National Medical Research Council Collaborative Research Grants NMRC-CBRG-0099-2015 and NMRC/OFIRG/0037/2017; Ministry of Education Academic Research Fund Tier 3 MOE2017-T3-1-002 and NUSMed-FoS Joint Research Program NUHSRO/2018/075/NUSMed-FoS/01 to S.S.; and NUS Research Scholarship to A.B. and M.Z.B.I. T.B. was supported by the Natural Science Foundation of China 31871076 and Shanghai Municipal Science and Technology Major Project 2018SHZDZX01, ZJLab, and Shanghai Center for Brain Science and Brain-Inspired Technology. The funder had no role in study design, data collection, or interpretation. We thank Dr. Susan Jones (University of Cambridge) and Dr. Serena M. Dudek (National Institute of Environmental Health Sciences) for the constructive comments on the manuscript.

The authors declare no competing financial interests.

*Correspondence should be addressed to Sreedharan Sajikumar at phssks@nus.edu.sg.

<https://doi.org/10.1523/JNEUROSCI.2885-20.2021>

Copyright © 2021 the authors

Introduction

Neuromodulation allows for the adaptation and reconfiguration of neuronal circuits in response to changing external stimuli and transitions in behavioral states (Marder, 2012). Activity-dependent modifications in synaptic strength, such as LTP or LTD, create highly coupled neuronal ensembles in the hippocampus that encode information and form memories, and are regulated by the action of neuromodulators (Palacios-Filardo and Mellor, 2019). The hippocampal subfield CA2, positioned between CA3 and CA1, is considered a modulatory gateway in the hippocampal circuitry (Benoy et al., 2018) with enriched expression of receptors for neuromodulators, such as oxytocin (H. J. Lee et al.,

2008) and vasopressin (Young et al., 2006), and afferent projections from neuromodulator-releasing nuclei, such as the substance P-releasing supramammillary nucleus (Borhegyi and Leranth, 1997; Chen et al., 2020), serotonergic median raphe nucleus, vasopressinergic paraventricular nucleus (Cui et al., 2013), and cholinergic medial septum and diagonal bands of Broca (Meibach and Siegel, 1977; Nyakas et al., 1987; Yoshida and Oka, 1995; Cui et al., 2013). The CA2 area also forms reciprocal connections projecting back to the supramammillary nucleus (Cui et al., 2013) and to the cholinergic nuclei of the medial septum–diagonal bands of Broca complex (Gaykema et al., 1991). In addition, neurons of the CA2 area are well integrated within the cortico-hippocampal network with direct innervation from entorhinal cortex layer II (EC LII) neurons (EC LII→CA2) terminating at the distal CA2 dendritic regions that express robust activity-dependent LTP (Chevalleyre and Siegelbaum, 2010). In contrast, the CA3 Schaffer collateral (SC) inputs that synapse onto the CA2 proximal dendritic region do not express canonical activity-dependent LTP induced by conventional high-frequency stimulation that is effective at CA3→CA1 synapses (Zhao et al., 2007). However, neuromodulators, such as substance P (Dasgupta et al., 2017), and agonists to the vasopressin 1b and oxytocin receptors (Pagani et al., 2015) have been shown to promote synaptic potentiation at the SC-CA2 synapses.

Among the hippocampal CA subfields, the CA2 stratum pyramidale has been shown to have the highest density of the acetylcholine synthesizing enzyme, choline acetyltransferase (ChAT)-positive punctate immunoprecipitates in the human hippocampal formation (Ransmayr et al., 1989). ChAT immunoreactivity is also found to be more concentrated in the CA2 and CA3 regions of the rat hippocampus (Ichikawa and Hirata, 1986; Orta-Salazar et al., 2014). The CA2 region also shows the highest expression of acetylcholinesterase (AChE) enzyme relative to other CA regions (Mellgren et al., 1977; Bakst and Amaral, 1984). In view of the reciprocal connectivity of CA2 with the cholinergic medial septum and diagonal bands of Broca, and the enriched expression of cholinergic marker enzymes, ChAT and AChE, in CA2 relative to other CA regions, we hypothesized that cholinergic modulation shapes synaptic plasticity in hippocampal CA2 neurons.

In the present study, we have investigated how synaptic plasticity is regulated in the hippocampal CA2 area on chemical stimulation of cholinergic receptors with the nonselective cholinergic agonist, carbachol (CCh). We observed that CCh-induced long-term depression (CCh-LTD) “primes” CA2 synapses for future LTP in a metaplastic manner. Metaplasticity refers to a higher-order form of synaptic plasticity in which activity-dependent modifications in synaptic strength at a given point in time are regulated by the previous history of synaptic or cellular activity (Abraham and Bear, 1996). We find that the metaplastic trigger by prior cholinergic receptor activation-induced LTD enables persistent LTP expression at EC-CA2 and SC-CA2 synapses subsequently subjected to stimuli otherwise subthreshold for the expression of lasting LTP. The CCh-primed persistent expression of LTP at EC-CA2 coexists with concomitant CCh-LTD at SC-CA2 synapses, and is dynamically downscaled by the modulation of SC-CA2 synaptic transmission, alluding to a heterosynaptic interplay between afferent SC stimulation and the metaplastic reinforcement of LTP at cortical inputs to CA2 neurons. Together, this study brings to light a previously unrecognized role for metaplasticity by cholinergic activation in the dynamic temporal regulation of synaptic efficacy in CA2 neurons, which could potentially mediate experience-dependent and behavioral state-dependent modulation of synaptic plasticity, and thereby learning and memory.

Materials and Methods

Animals and preparation of hippocampal slices. For electrophysiological experiments, a total of 200 acute hippocampal slices were used from 100 young adult male Wistar rats (P35–P49). All animals were kept under 12 h light/dark cycle with food and water available *ad libitum*. Animal procedures were performed in accordance with the protocols R15-0200 and R16-0135, approved by the Institutional Animal Care and Use Committee of the National University of Singapore. Rats were anesthetized using CO₂ and thereafter decapitated, following which brains were removed and hippocampi quickly isolated in ACSF maintained at 4°C and pH 7.3. The composition (in mM) of ACSF (Dasgupta et al., 2017) is as follows: 124 NaCl, 2.5 KCl, 2 MgCl₂, 2 CaCl₂, 1.25 NaH₂PO₄, 26 NaHCO₃, and 17 D-glucose, equilibrated with 95% O₂ and 5% CO₂ (carbogen). Using a manual tissue chopper, transverse hippocampal slices with a thickness of 400 μm were prepared from the isolated hippocampi (right/left). Slices were then placed on a nylon net of an interface-type slice recording chamber (Scientific Systems Design) and incubated for a minimum of 2–3 h at 32°C before placing recording and stimulating electrodes. The ACSF flow rate to the chamber was maintained at 1 ml/min. Anesthetization, dissection, and transfer of slices to the chamber were performed quickly and did not exceed an average duration of 5 min (Shetty et al., 2015).

Extracellular field potential recording. Three monopolar lacquer-insulated stainless-steel electrodes (5 MΩ; AM Systems) were positioned in the hippocampal area CA2 for the two-pathway experiments, and two monopolar lacquer-insulated stainless-steel electrodes were placed in area CA2 for the single-pathway experiments. Briefly, for the two-pathway experiments, two stimulating electrodes, one stimulating the SC fibers (CA3→CA2) and the other stimulating the entorhinal cortical fibers (EC LII→CA2) onto CA2, were positioned at the proximal and distal sites of the CA2 area, respectively. Field excitatory postsynaptic potentials (fEPSPs) on stimulation of proximal and distal inputs were recorded from the midline of proximal-distal CA2 dendritic region (Fig. 1A). The same applies for the single-pathway experiments performed in this study, with the exception that, in addition to the recording electrode at the CA2 dendritic region, only one stimulating electrode was positioned which stimulates either the proximal SC fibers or the distal EC fibers onto CA2.

The recorded signals were amplified by a differential amplifier (model 1700; AM Systems), digitized using a CED 1401 analog-to-digital converter (Cambridge Electronic Design), and monitored online with Intracell software (iF) where the initial slope function (millivolts per millisecond) of the fEPSP is measured for analysis. The independence of the EC and SC synaptic inputs onto CA2 was confirmed using a cross-input paired-pulse facilitation protocol with an interstimulus interval of 50 ms similar to our previous study (Dasgupta et al., 2017). The absence of paired-pulse facilitation indicated that the two stimulating electrodes activated independent synaptic inputs (Dasgupta et al., 2017). For the experiment in Figure 2B, two stimulating electrodes, one stimulating the SC fibers (CA3→CA1) and the other stimulating the EC fibers (EC LIII→CA1) onto CA1, were positioned at the CA1 stratum radiatum (SR) and CA1 stratum lacunosum-moleculare (SLM), respectively, and fEPSPs were recorded from the CA1 dendritic region on stimulation of the proximal SC and distal EC inputs (Fig. 2A).

After the preincubation period of 2–3 h for recovery of slices placed in the interface chamber following dissection, an input-output relation (afferent stimulation intensity vs fEPSP slope) for each stimulated synaptic input was generated to determine the test stimulation strength which was set to obtain an fEPSP response with 40% of the maximal fEPSP slope value. At this stimulus intensity, a stable baseline was recorded for 30 min before application of pharmacological agents or tetanizing stimuli. The basal stimulation consists of four sweeps of 0.2 Hz biphasic constant current pulses (pulse duration, 0.1 ms per polarity) at each time point (Shetty et al., 2015). For early LTP (E-LTP) induction, a “weak” tetanization (WTET) protocol consisting of a single train of high-frequency stimulation of 21 pulses at 100 Hz (pulse duration, 0.2 ms per polarity) was delivered (Shetty et al., 2015). The “strong” tetanization (STET) protocol consisted of three trains of high-frequency stimulation of 100 pulses at 100 Hz (pulse duration, 0.2 ms per polarity) with an intertrain interval of 10 min (Shetty et al., 2015). Paired-pulse stimulation experiments in Figures 3A, C and 8C were performed by delivering

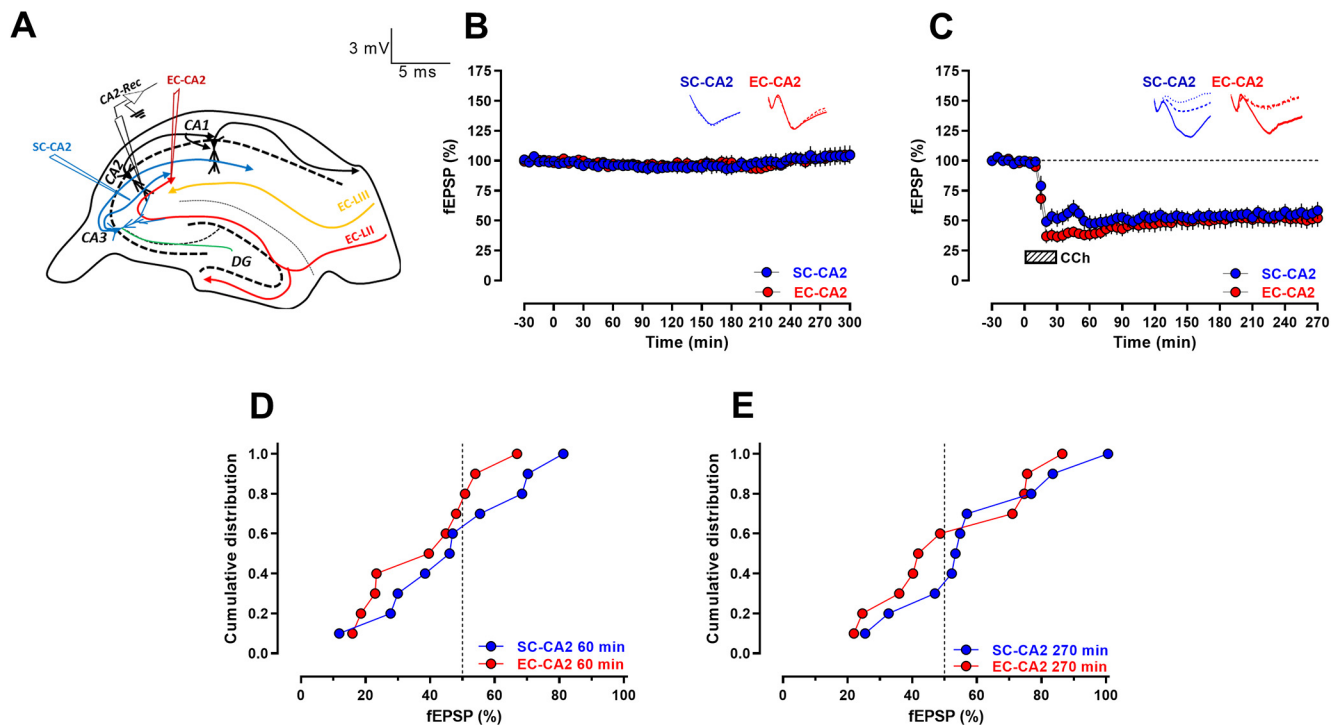


Figure 1. Nonselective cholinergic receptor agonist, CCh, triggers long-lasting synaptic depression at EC and SC synaptic inputs to CA2 neurons. **A**, Schematic diagram represents the location of electrodes in the acute hippocampal slices for extracellular field electrophysiology recordings from the CA2 region. Blue inverted triangle represents the placement of electrode in the SR stimulating the SC afferents to CA2. Red inverted triangle represents the location of electrode in the SLM stimulating the EC afferents to CA2. Black inverted triangle represents the position of the recording electrode in the CA2 dendritic region. **B**, Control experiments at basal synaptic stimulation frequency indicate the long-lasting stability of SC-CA2 and EC-CA2 fEPSP recordings in this study ($n = 6$). **C**, Bath application of $50 \mu\text{M}$ CCh for 30 min after a 30 min stable baseline induced a long-lasting synaptic depression (CCh-LTD) at SC and EC inputs to CA2 at basal synaptic stimulation, lasting for 4 h after CCh application ($n = 10$). Data are mean \pm SEM. Analog traces are representative SC-CA2 (blue) and EC-CA2 (red) fEPSPs within the initial 30 min baseline recording (closed line) before CCh application, and 60 min (dotted line) and 270 min (hatched line) after baseline. **D**, **E**, Summary data with cumulative frequency distribution plots of SC-CA2 and EC-CA2 fEPSP (%) values from **C** at 60 min (**D**) and 270 min (**E**) into CCh application. Calibration for analog traces: **B**, **C**, 3 mV, 5 ms.

pairs of stimulation pulses with an interstimulus interval of 10, 30, 50, 70, 100, 150, and 250 ms, to individual synaptic inputs at specified time points (described in Results) of the fEPSP recording for the respective experiments. All field potential recordings in this study were performed in the absence of application of GABA receptor antagonists similar to our previous studies (Dasgupta et al., 2017, 2020), and therefore reflect responses from hippocampal neurons with intact inhibitory transmission.

Pharmacology. The nonselective cholinergic receptor agonist, (2-hydroxyethyl)trimethylammonium chloride carbamate (CCh; C4382; Sigma-Aldrich), was prepared as 50 mM stock in deionized water and diluted to a final concentration of $50 \mu\text{M}$ in ACSF. Protein synthesis inhibitor, emetine dihydrochloride hydrate (emetine; E2375; Sigma-Aldrich), was prepared as 20 mM stock in deionized water and diluted to $20 \mu\text{M}$ final concentration in ACSF. The NMDAR antagonist, D-AP5 (0106; Tocris Bioscience), was stored at -20°C as 50 mM stock prepared in deionized water and diluted before application to a final concentration of $50 \mu\text{M}$ in ACSF. The M1 muscarinic receptor antagonist, 5,11-dihydro-11-[(4-methyl-1-piperazinyl)acetyl]-6H-pyrido[2,3-*b*] [1,4] benzodiazepin-6-one dihydrochloride (pirenzepine; 1071; Tocris Bioscience), was prepared as 10 mM stock in deionized water and diluted to a final concentration of $0.5 \mu\text{M}$ in ACSF. The M2 muscarinic receptor antagonist, 11-[[2-[(diethylamino)methyl]-1-piperidinyl]acetyl]-5,11-dihydro-6H-pyrido[2,3-*b*] [1,4] benzodiazepin-6-one (AF-DX 116; 1105; Tocris Bioscience), was prepared as 10 mM stock in DMSO, stored at -20°C , and diluted before application to a final concentration of $2 \mu\text{M}$ in ACSF. The M3 muscarinic receptor antagonist, 1,1-dimethyl-4-diphenylacetoxypiperidinium iodide (4-DAMP; 0482; Tocris Bioscience), was prepared as 10 mM stock in DMSO, stored at -20°C , and diluted before application to a final concentration of $1 \mu\text{M}$ in ACSF. The nonselective muscarinic receptor antagonist, (endo,syn)-(\pm)-3-(3-hydroxy-1-oxo-2-phenylpropoxy)-8-methyl-8-(1-methylethyl)-8-azoniabicyclo[3.2.1]octane

bromide (atropine; 0692; Tocris Bioscience), was prepared as 5 mM stock in deionized water and diluted to a final concentration of $1 \mu\text{M}$ in ACSF. The noncompetitive nicotinic receptor antagonist, *N*,2,3,3-tetramethylbicyclo[2.2.1]heptan-2-amine hydrochloride (mecamylamine; 2843; Tocris Bioscience), was prepared as 20 mM stock in deionized water and diluted to a final concentration of $20 \mu\text{M}$ in ACSF. The concentrated pharmacological agent stock solutions were diluted in ACSF to their respective final concentrations shortly before application, after which the pharmacological agent-containing ACSF was saturated with carbogen and bath-applied. Detailed descriptions of the duration and time point of application for individual pharmacological agents are provided in Results. Where DMSO was used to prepare the stock solution, the final DMSO concentration in the working solution was kept $\leq 0.1\%$, a concentration shown in previous studies to not affect basal synaptic transmission (Navakkode et al., 2004). Light-sensitive pharmacological agents were shielded from exposure to light during storage and bath application.

Data presentation and statistical analysis. The fEPSP values are represented as the mean of normalized fEPSP slope function (percentage of baseline) \pm SEM. Nonparametric tests were used for the statistical analysis as the sample size per series did not always guarantee a Gaussian normal distribution of the data. When comparing between two time points within the same group of data, the Wilcoxon signed-rank test (Wilcoxon test) was used for analysis. When comparing between two different groups of data at a specific time point, the values were analyzed using the Mann-Whitney *U* test (*U* test). When three different groups are compared against each other at a specific time point, the mean normalized fEPSP (%) values were analyzed using the Kruskal-Wallis test followed by Dunn's multiple comparisons *post hoc* analysis. Kolmogorov-Smirnov test was used to compare cumulative frequency distributions. Paired-pulse ratio is calculated as the ratio (P2/P1) of the slope function of the second fEPSP to that of the first for pairs of stimulation pulses delivered with the specified interstimulus intervals. Kruskal-Wallis test followed by Dunn's

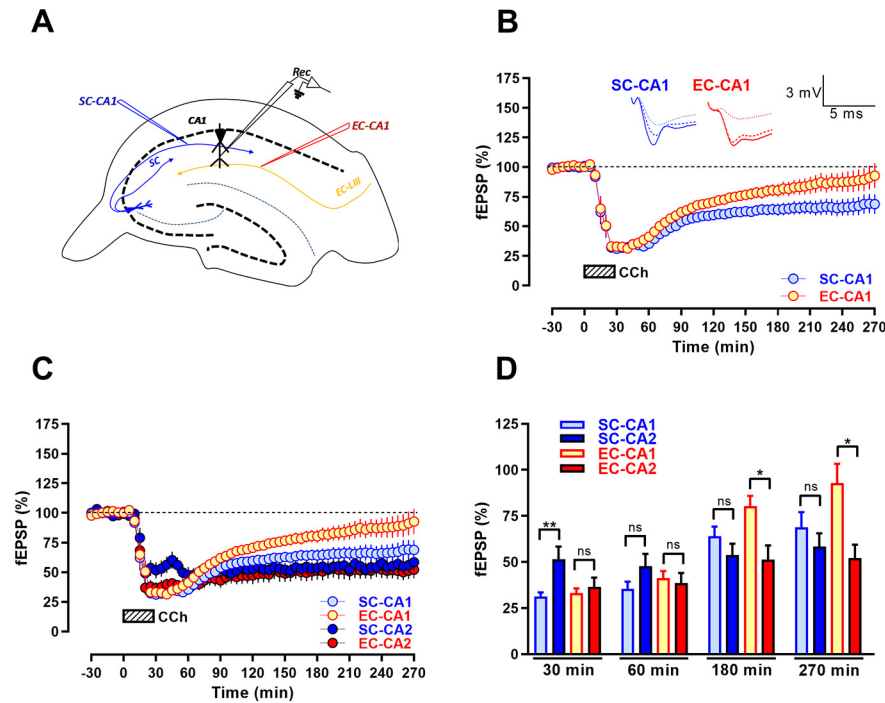


Figure 2. Comparison of CCh-LTD between hippocampal CA1 and CA2 synapses. **A**, Schematic diagram represents the location of electrodes in the acute hippocampal slices for extracellular field electrophysiology recordings from the CA1 region. Blue inverted triangle represents the placement of electrode in the SR stimulating the SC afferents to CA1 (SC-CA1). Red inverted triangle represents the location of electrode in the SLM stimulating the EC layer III (EC-LIII) afferents to CA1 (EC-CA1). Black inverted triangle represents the position of the recording electrode in the CA1 dendritic region. **B**, Bath application of CCh ($50 \mu\text{M}$) for 30 min after a 30 min stable baseline induced a long-lasting synaptic depression at SC-CA1, lasting up to 270 min into CCh application, while synaptic responses at EC-CA1 reversed to levels not significantly different from its baseline levels by 210 min into CCh application ($n = 10$). **C**, Superimposition of CCh-LTD at CA2 synapses (data from Fig. 1C) and CA1 synapses (data from **B**) for the ease of comparison. **D**, Summary bar chart represents fEPSP (%) at 30, 60, 180, and 270 min into CCh application compared between SC-CA1 and SC-CA2 synapses, and between EC-CA1 and EC-CA2 synapses. Significant differences between the two groups: $*p < 0.05$; $**p < 0.01$; Not significant: ns, $p > 0.05$; U test. Data are mean \pm SEM. **B**, Analog traces are representative SC-CA1 (blue) and EC-CA1 (red) fEPSPs within the initial 30 min baseline recording (closed line) before CCh application, and 60 min (dotted line) and 270 min (hatched line) after baseline. Calibration: **B**, 3 mV, 5 ms.

multiple comparisons *post hoc* analysis was used to compare paired-pulse ratios between three groups. Differences at $p < 0.05$ were considered statistically significant. Prism (GraphPad Software) was used to plot the graphs and for the statistical analysis. Detailed description of the statistical analysis for individual experiments is provided in Results.

Results

Cholinergic receptor activation triggers protein synthesis-dependent and NMDAR-independent LTD at both EC- and SC-CA2 synapses

Based on our hypothesis that cholinergic modulation could shape synaptic plasticity in hippocampal CA2 neurons, we first sought to investigate changes in synaptic efficacy along the proximo-distal dendritic axis of neurons in area CA2 owing to cholinergic receptor activation. To this end, we performed extracellular field potential recordings in acute rat hippocampal slices and thereby recorded synaptic activity from a population of CA2 neurons as fEPSPs on stimulation of the distal EC-CA2 and the proximal SC-CA2 synapses. Control recordings were performed at basal stimulation frequency (0.2 Hz) that resulted in stable synaptic responses for 5 h after a baseline of 30 min at EC-CA2 and SC-CA2 synapses (Fig. 1B, EC-CA2, red circles, 300 min: Wilcoxon test, $p = 0.6875$; SC-CA2, blue circles, 300 min: Wilcoxon test, $p = 0.6875$), thus demonstrating the stability of the field potential recordings performed in this study. To probe the effect of

cholinergic stimulation in CA2 neurons, the nonselective cholinergic receptor agonist, CCh ($50 \mu\text{M}$), was bath-applied for 30 min after taking a baseline recording of 30 min (Fig. 1C), resulting in a sustained synaptic depression (CCh-LTD) that lasted for 4 h after CCh application at both EC-CA2 (Fig. 1C, red circles, 270 min: Wilcoxon test, $p = 0.0020$) and SC-CA2 synapses (Fig. 1C, blue circles, 270 min: Wilcoxon test, $p = 0.0039$). A previous study has shown that activity-dependent LTD in response to low-frequency electrical stimulation exhibits a heterogeneous expression pattern in CA2 neurons in the rat hippocampus (Zhao et al., 2007). The cumulative frequency distribution of fEPSP (%) values from Figure 1C, 60 and 270 min into CCh application, is shown in Figure 1D and Figure 1E, respectively. The data indicate some form of heterogeneity, at a minor level, for CCh-LTD displayed by EC- and SC-CA2 synapses, wherein CA2 synapses in a few experiments displayed a near reversal to baseline values over time (Fig. 1E). However, in the majority of experiments, the EC- and SC-CA2 synapses remained significantly depressed on cholinergic activation by CCh application. We also noted that the cumulative frequency distribution of field potentials between EC and SC inputs to CA2 at 60 and 270 min into CCh application is not significantly different (Fig. 1D, Kolmogorov–Smirnov test, $p = 0.7591$; Fig. 1E, Kolmogorov–Smirnov test, $p = 0.7591$).

Next, we sought to explore how the CCh-induced depression at synapses in area CA2 compares with that in area

CA1. To determine this, we recorded synaptic responses from the hippocampal CA1 region on independently stimulating CA1 SR where SCs terminate on CA1 neurons (SC-CA1), and CA1 SLM where axons primarily from EC layer III terminate on CA1 neurons (EC-CA1) (Fig. 2A). Briefly, CCh ($50 \mu\text{M}$) was bath-applied for a duration of 30 min after a 30 min stable baseline and synaptic responses from SC-CA1 and EC-CA1 were continued to be recorded up to 4 h after CCh application at basal stimulation frequency throughout as shown in Figure 2B. We observed that, similar to SC-CA2 synapses, synaptic responses in CA1 SR (SC-CA1) displayed sustained CCh-induced synaptic depression up to 4 h after CCh application (Fig. 2B, blue circles, 270 min: Wilcoxon test, $p = 0.0059$). However, unlike EC-CA2, which remained significantly depressed up to 270 min into CCh application, synaptic responses at CA1 SLM (EC-CA1) returned to levels not significantly different from its baseline levels by 210 min into CCh application (Fig. 2B, yellow circles, 210 min: Wilcoxon test, $p = 0.0645$). The CCh-induced depression has also been previously reported to be expressed differently between the SR and SLM of CA1 area in that CA1 SR displays greater CCh-induced synaptic depression compared with CA1 SLM (Hasselmo and Schnell, 1994). The effect of CCh on synaptic responses in SR and SLM of CA2 area (data from Fig. 1C) and CA1 area (data from Fig. 2B) is compared against each other at

30, 60, 180, and 270 min into CCh application in Figure 2D. Together, the summarized data in Figure 2D suggest that, while the maintenance of LTD in response to cholinergic receptor activation differs between CA2 SLM (EC-CA2) and CA1 SLM (EC-CA1) (Fig. 2D, 180 min: *U* test, $p = 0.0232$, 270 min: *U* test, $p = 0.0115$), it is similar between CA2 SR (SC-CA2) and CA1 SR (SC-CA1) (Fig. 2D, 180 min: *U* test, $p = 0.2475$, 270 min: *U* test, $p = 0.3930$), and the CCh-induced immediate depression is significantly greater at SC-CA1 compared with SC-CA2 synapses (Fig. 2D, 30 min: *U* test, $p = 0.0052$), while it does not significantly vary between EC-CA1 and EC-CA2 synapses (Fig. 2D, 30 min: *U* test, $p = 0.6305$).

We also analyzed the paired-pulse ratio at both EC-CA2 (Fig. 3A,B) and SC-CA2 (Fig. 3C,D) before CCh application during the 30 min baseline recording (control) and 60 min into CCh application to determine whether CCh-LTD has a presynaptic or a postsynaptic locus of expression. Pairs of stimulation pulses with an interstimulus interval of 10, 30, 50, 70, 100, 150, and 250 ms were delivered before CCh application and 60 min into CCh application. We observed that, for 10 ms interstimulus interval, the paired-pulse ratio at EC-CA2 60 min into CCh application was significantly higher than the control paired-pulse ratio before CCh application (Fig. 3A, Wilcoxon test, $p = 0.0156$). However, at higher interstimulus intervals, the paired-pulse ratio at EC-CA2 60 min into CCh application was not significantly different from that before CCh application (Fig. 3A, Wilcoxon test, interstimulus intervals 30 ms: $p = 0.9453$, 50 ms: $p = 0.3828$, 70 ms: $p = 0.1016$, 100 ms: $p = 0.1953$, 150 ms: $p = 0.9453$, 250 ms: $p = 0.9453$). The percent paired-pulse ratio at 10 ms interstimulus interval in EC-CA2 normalized by the average control paired-pulse ratio is presented in Figure 3B and shows a significant increase of $34.05 \pm 8.154\%$ at 60 min into CCh application (Fig. 3B, Wilcoxon test, $p = 0.0156$). However, the paired-pulse ratio at SC-CA2 was not significantly different before CCh and 60 min into CCh application, at all the interstimulus intervals tested (Fig. 3C, Wilcoxon test, interstimulus intervals 10 ms: $p = 0.1172$, 30 ms: $p = 0.2422$, 50 ms: $p = 0.5469$, 70 ms: $p = 0.3125$, 100 ms: $p = 0.8125$, 150 ms: $p = 0.9999$, 250 ms: $p = 0.3828$). This suggests that no significant changes in presynaptic release probability are induced at SC-CA2 synapses 60 min into CCh application. The percent paired-pulse ratio at 10 ms interstimulus interval in SC-CA2 normalized by the average control paired-pulse ratio is presented in Figure 3D and shows no significant change between control and CCh groups (Fig. 3D, Wilcoxon test, $p = 0.1172$). An increase in paired-pulse ratio in CA2 neurons after CCh application has been previously reported in mice by means of whole-cell recordings of CA2 pyramidal neurons where a significantly greater paired-pulse

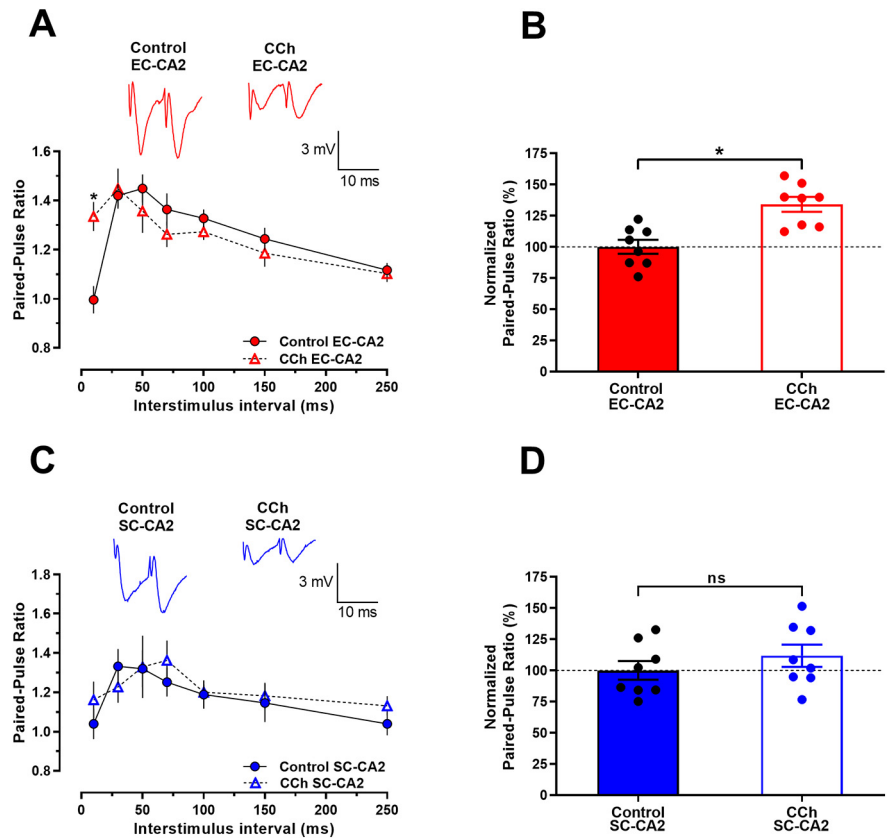


Figure 3. Paired-pulse ratio at different interstimulus intervals for EC-CA2 and SC-CA2 synapses, during baseline and 60 min into CCh application. **A**, Paired-pulse ratio at EC-CA2 before CCh application during the 30 min baseline recording (control) and 60 min into CCh application (CCh) recorded for interstimulus intervals of 10, 30, 50, 70, 100, 150, and 250 ms ($n = 8$). Paired-pulse ratio at 10 ms interstimulus interval in EC-CA2 60 min into CCh application is significantly higher than control paired-pulse ratio before CCh application. **B**, Paired-pulse ratio (%) at 10 ms interstimulus interval in EC-CA2 normalized by the average control paired-pulse ratio shows a significant increase for 60 min into CCh application compared with control. **C**, Paired-pulse ratios at SC-CA2 were not significantly different before CCh (control) and 60 min into CCh application (CCh) at 10, 30, 50, 70, 100, 150, and 250 ms interstimulus intervals ($n = 8$). **D**, Paired-pulse ratio (%) at 10 ms interstimulus interval in SC-CA2 normalized by the average control paired-pulse ratio shows no significant change between control and CCh groups. Data are mean \pm SEM. Differences between groups: * $p < 0.05$; ns, not significant, $p > 0.05$ (Wilcoxon test). Representative analog traces depict EC-CA2 (red) and SC-CA2 (blue) fEPSPs for the paired-pulse stimulation at 10 ms interstimulus interval. Calibration: **A**, **C**, 3 mV, 10 ms.

ratio of evoked EPSCs was observed after CCh (10 μM) application, reflecting a decrease in presynaptic glutamate release probability associated with CCh-induced depression of excitatory synaptic transmission onto CA2 pyramidal neurons (Robert et al., 2020). It is intriguing that, in the present study, the increase in paired-pulse ratio at EC-CA2, 60 min into CCh application, was only observed at the 10 ms interstimulus interval and not at higher interstimulus intervals. It must be noted here that the paired-pulse stimulation experiments in the present study were conducted under conditions that did not block spontaneous synaptic events or inhibitory synaptic transmission. Overall, given that the increase in paired-pulse ratio at EC-CA2 synapses on CCh application was only displayed at 10 ms interstimulus interval, the observed effects likely reflect only very short-term modifications of presynaptic release mechanisms, possibly shaped by cholinergic stimulation-induced intracellular calcium release patterns (Seymour-Laurent and Barish, 1995) or other CCh-induced modulatory mechanisms that remain to be determined. Not being the primary focus of the present study, this was not further explored and is open to future investigation.

Next, the persistence of CCh-induced synaptic depression was shown to be protein synthesis-dependent as bath application of the protein synthesis inhibitor, emetine (20 μM), significantly attenuated the late maintenance of synaptic depression at CA2

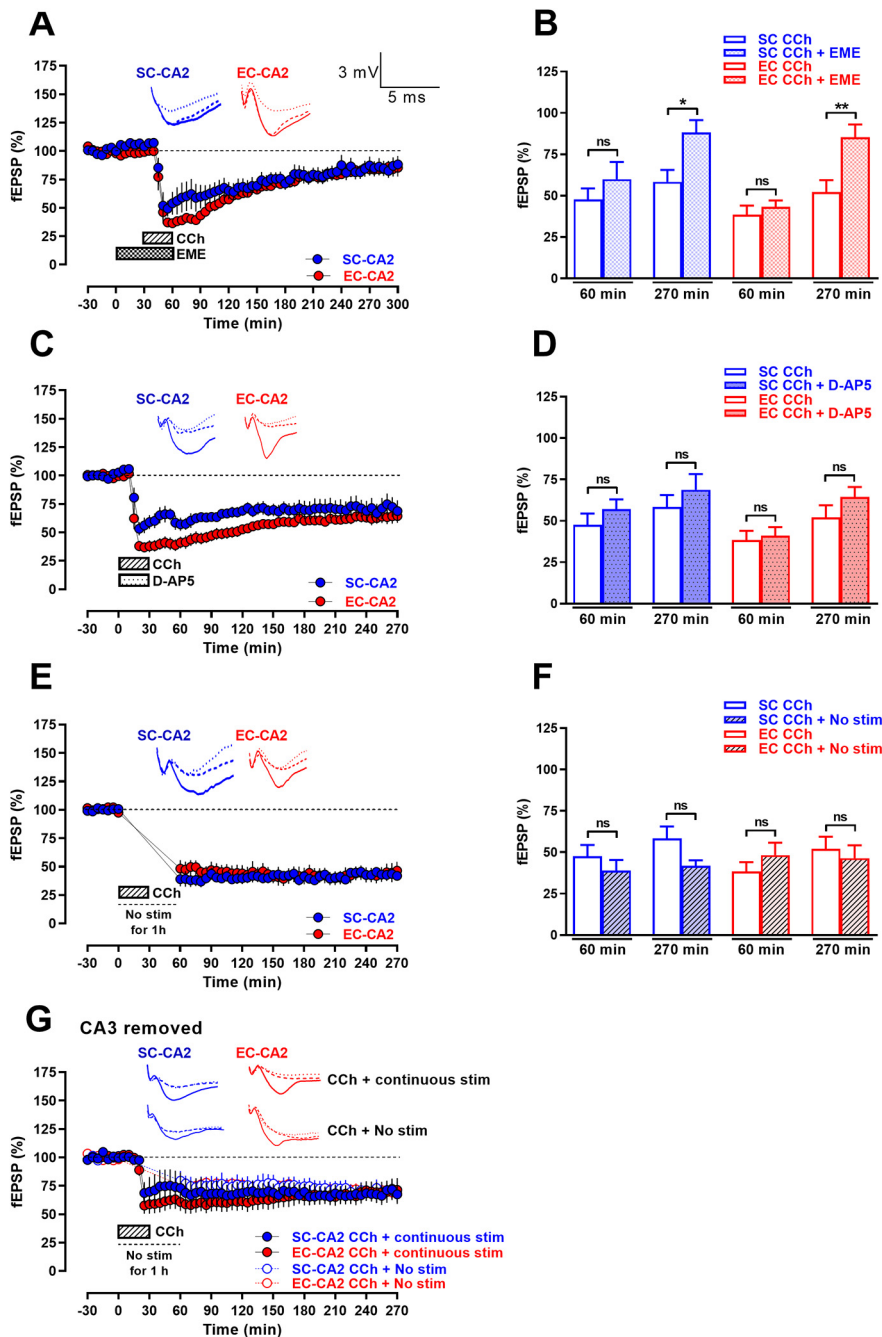


Figure 4. Persistence of CCh-LTD at CA2 synapses requires protein synthesis but is independent of NMDAR activation and continuous afferent synaptic drive. **A**, Bath application of the protein synthesis inhibitor, emetine (EME; 20 μ M), attenuates the late phase of CCh-LTD at CA2 synapses ($n = 7$). **B**, Summary bar chart comparing fEPSP (%) at 60 min (acute CCh-LTD) and 270 min (sustained CCh-LTD) into CCh application between Figure 1C (CCh alone) and Figure 4A (CCh + emetine). **C**, Bath application of the NMDAR antagonist, D-AP5 (50 μ M), does not abrogate CCh-LTD that persists into the late phase ($n = 8$). **D**, Summary bar chart comparing fEPSP (%) at 60 and 270 min into CCh application between Figure 1C (CCh alone) and Figure 4C (CCh + D-AP5). **E**, In intact hippocampal slices, suspension of basal test stimulus for 1 h (No stim) at EC-CA2 and SC-CA2 does not block CCh-LTD and displays stable synaptic depression into the late phase ($n = 6$). **F**, Summary bar chart comparing fEPSP (%) at 60 and 270 min into CCh application between Figure 1C (CCh alone) and Figure 4E (CCh + No stim). **G**, In hippocampal slices with CA3 surgically removed, suspension of basal test stimulus for 1 h (CCh + No stim) at EC-CA2 and SC-CA2 also leads to significant synaptic depression persisting into the late phase (open circles, $n = 7$), that is comparable with CCh-LTD observed at EC-CA2 and SC-CA2 without suspension of basal test stimulus (CCh + continuous stim) (filled circles, $n = 7$). Data are mean \pm SEM. Significant differences between two groups: * $p < 0.05$; ** $p < 0.01$; Not significant: ns, $p > 0.05$; U test. Analog traces are representative EC-CA2 (red) and SC-CA2 (blue) fEPSPs within 30 min before CCh application (closed line), at 60 min into CCh application (dotted line), and at 270 min into CCh application (hatched line). **G**, Top, Analog traces represent experiments with uninterrupted test stimulation. Bottom, Traces from experiments where test stimulation was paused for 1 h. Calibration **A**, **C**, **E**, **G**, 3 mV, 5 ms.

synapses in response to CCh (Fig. 4A). As shown in Figure 4A, emetine was applied for a total of 1 h (30 min before coapplication with CCh for another 30 min), and this resulted in fEPSPs at EC- and SC-CA2 synapses gradually returning to levels not significantly different from their respective baseline recordings by 265 min into emetine application for EC-CA2 (Fig. 4A, red circles, 265 min: Wilcoxon test, $p = 0.1094$) and by 240 min into emetine application for SC-CA2 (Fig. 4A, blue circles, 240 min: Wilcoxon test, $p = 0.2969$). Figure 4B represents the fEPSP (%) values at 60 and 270 min into CCh application compared between Figure 4A (CCh + emetine) and Figure 1C (CCh alone) at the specific time points. The experiments in Figures 4A and 1C were not strictly interleaved within the same time frame, but both experiments used similar conditions for preparation of hippocampal slices and long-term electrophysiological recordings. As shown in Figure 4B, the acute CCh-LTD (60 min into CCh application) was comparable with and without emetine (EC-CA2, U test, $p = 0.8125$; SC-CA2, U test, $p = 0.4173$). However, the late phase of CCh-LTD (270 min into CCh application) was significantly attenuated in the presence of emetine compared with the late phase of LTD with CCh alone at both EC-CA2 (Fig. 4B, U test, $p = 0.0097$) and SC-CA2 synapses (Fig. 4B, U test, $p = 0.0185$). As shown in Figure 4A, by the end of the recording period (270 min into CCh application), EC-CA2 and SC-CA2 fEPSPs attained mean fEPSP (%) values of $85.30 \pm 7.766\%$ and $88.24 \pm 7.428\%$, respectively, with emetine application, and were also not significantly different compared with their respective baseline levels (Fig. 4A, EC-CA2, red circles, 300 min: Wilcoxon test, $p = 0.1563$; SC-CA2, blue circles, 300 min: Wilcoxon test, $p = 0.3750$). Overall, the data and analyses in Figure 4A, B suggest that emetine significantly decreases the magnitude of the late phase of CCh-LTD but does not appear to completely eliminate it as a slight depression is still displayed at the end of the recording period, although not statistically significant.

The LTD induced by CCh, however, was not NMDAR-dependent as coapplication of the NMDAR antagonist, D-AP5 (50 μ M), with CCh did not attenuate CCh-LTD at either synaptic inputs to CA2 with fEPSPs significantly lower than baseline levels even by

270 min into CCh application (Fig. 4C, EC-CA2, red circles, 270 min: Wilcoxon test, $p = 0.0078$; SC-CA2, blue circles, 270 min: Wilcoxon test, $p = 0.0234$). Figure 4D compares fEPSP (%) values from Figure 4C (CCh + D-AP5) against Figure 1C (CCh alone), at 60 and 270 min into CCh application, and shows that fEPSPs for both acute CCh-LTD (60 min) and sustained CCh-LTD (270 min) in Figures 1C and 4C are not significantly different from each other (Fig. 4D, EC-CA2, 60 min: U test, $p = 0.5148$, 270 min: U test, $p = 0.1728$; SC-CA2, 60 min: U test, $p = 0.3154$, 270 min: U test, $p = 0.3599$). We further determined that CCh-LTD at CA2 synapses was independent of continuous afferent synaptic drive as we observed a significant and lasting LTD at EC- and SC-CA2 synapses even when test stimulation was suspended for 1 h (30 min during application of CCh and 30 min immediately following CCh application) (Fig. 4E). As demonstrated in Figure 4E, both EC- and SC-CA2 displayed significant synaptic depression compared with their respective baseline recordings, despite the 1 h pause in test stimulation (EC-CA2, red circles, 270 min: Wilcoxon test, $p = 0.0313$; SC-CA2, blue circles, 270 min: Wilcoxon test, $p = 0.0313$). Figure 4F compares fEPSP (%) values from Figure 4E (CCh + suspension of test stimulus) against Figure 1C (CCh alone), at 60 and 270 min into CCh application, and shows that fEPSPs for both acute CCh-LTD (60 min) and sustained CCh-LTD (270 min) in Figure 1C and 4E are not significantly different from each other (Fig. 4F, EC-CA2, 60 min: U test, $p = 0.4278$, 270 min: U test, $p = 0.7925$; SC-CA2, 60 min: U test, $p = 0.4278$, 270 min: U test, $p = 0.1179$). Although CCh-LTD was displayed at CA2 synapses despite the pause in test stimulation as demonstrated in Figure 4E, it does not confirm that CCh-LTD at CA2 synapses is fully activity-independent as CCh application has been shown to induce oscillatory activity in CA3 pyramidal cells even in the absence of electrical stimulation (Williams and Kauer, 1997). To rule out the role of CCh-induced CA3 neuronal activity in the observed CCh-LTD at CA2 synapses, we monitored CCh-LTD at EC- and SC-CA2 synapses with pause (Fig. 4G, open circles; CCh + No stimulation for 1 h) and without pause in test stimulation (Fig. 4G, filled circles; CCh + continuous stimulation) in hippocampal slices with the CA3 region surgically removed (Scheiderer et al., 2006). Despite the removal of CA3 region, a significant and lasting LTD was observed at EC- and SC-CA2 synapses compared with their respective baseline levels, when CCh was bath-applied for 30 min after a 30 min stable baseline, in experiments where test stimulation was not paused (Fig. 4G, EC-CA2, red filled circles, 270 min: Wilcoxon test, $p = 0.0469$; SC-CA2, blue filled circles, 270 min: Wilcoxon test, $p = 0.0156$). Moreover, even when test stimulation was suspended briefly for 1 h (30 min during application of CCh and 30 min immediately following CCh application) in hippocampal slices with CA3 removed, both EC- and SC-CA2 synapses still displayed a significant and persistent CCh-LTD compared with their individual baseline levels (Fig. 4G, EC-CA2, red open circles, 270 min: Wilcoxon test, $p = 0.0156$; SC-CA2, blue open circles, 270 min: Wilcoxon test, $p = 0.0313$). The persistent CCh-LTD so observed in hippocampal slices with CA3 removed, with (Fig. 4G, open circles) and without (Fig. 4G, filled circles) pause in test stimulation, was also not significantly different compared against each other at both EC-CA2 (Fig. 4G, 270 min: U test, $p = 0.9656$) and SC-CA2 (Fig. 4G, 270 min: U test, $p = 0.8718$) synapses. Together, these results suggest that CCh-LTD at CA2 synapses is independent of CCh-induced CA3 neuronal activity as well. However, it does not completely rule out activity dependence of CCh-LTD at CA2 synapses as CCh application has also been

observed to induce spontaneous burst firing of action potentials in CA2 pyramidal cells even in the absence of synaptic transmission (Robert et al., 2020). Whether or not activity by CCh-induced spontaneous firing of CA2 pyramidal cells has any role in mediating the observed CCh-LTD at CA2 synapses remains to be determined.

Differential role for mAChRs and nAChRs in facilitating CCh-LTD at CA2 synapses

Acetylcholine (ACh) exerts its effects on neural activity by acting on ionotropic nicotinic ACh receptors (nAChRs) and metabotropic muscarinic ACh receptors (mAChRs) (Brown, 2019). Given the expression of cholinergic receptors belonging to both ACh receptor classes in the CA2 region (Wada et al., 1989; Seguela et al., 1993; Levey et al., 1995), we were intrigued to understand the relative roles played by the different cholinergic receptors in mediating CCh-LTD at CA2 synapses. To this end, the effects of different cholinergic receptor antagonists on CCh-LTD at CA2 synapses were explored and compared against CCh-LTD within the same time frame in interleaved control experiments without receptor antagonists (Fig. 5A–E). It was observed that the application of the selective muscarinic M1 receptor antagonist, pirenzepine ($0.5 \mu\text{M}$), for a total duration of 50 min (20 min before coapplication with CCh for another 30 min), resulted in fEPSPs returning to levels not significantly different from their individual baseline values by 100 and 210 min into CCh application at EC- and SC-CA2 synapses, respectively (Fig. 5A, EC-CA2, red open circles, 120 min: Wilcoxon test, $p = 0.0742$; SC-CA2, blue open circles, 230 min: Wilcoxon test, $p = 0.0742$). This attenuation of fEPSPs in the presence of pirenzepine (Fig. 5A, open circles) was also significantly different compared with both the early and late phases of CCh-LTD in interleaved control experiments without pirenzepine (Fig. 5A, filled circles) at EC-CA2 (Fig. 5A, 60 min into CCh: U test, $p = 0.0025$; 250 min into CCh: U test, $p = 0.0152$) and SC-CA2 synapses (Fig. 5A, 60 min into CCh: U test, $p = 0.0025$; 250 min into CCh: U test, $p = 0.0055$). However, application of the selective muscarinic M2 receptor antagonist, AF-DX 116 ($2 \mu\text{M}$), for a total duration of 50 min (20 min before coapplication with CCh for 30 min), did not abrogate the maintenance of CCh-LTD at CA2 synapses with fEPSPs significantly depressed from its baseline values until the end of the recording period at both EC- and SC-CA2 synapses (Fig. 5B, EC-CA2, red open circles, 270 min: Wilcoxon test, $p = 0.0156$; SC-CA2, blue open circles, 270 min: Wilcoxon test, $p = 0.0313$). The depression of fEPSPs so observed in the presence of AF-DX 116 (Fig. 5B, open circles) was also not significantly different compared with CCh-LTD in interleaved control experiments without AF-DX 116 (Fig. 5B, filled circles) at EC-CA2 (Fig. 5B, 60 min into CCh: U test, $p = 0.2785$; 250 min into CCh: U test, $p = 0.9305$) and SC-CA2 synapses (Fig. 5B, 60 min into CCh: U test, $p = 0.9203$; 250 min into CCh: U test, $p = 0.2754$). This suggests that muscarinic M2 receptor activation does not play a significant role in mediating CCh-LTD at CA2 synapses. Interestingly, application of the muscarinic M3 receptor antagonist, 4-DAMP ($1 \mu\text{M}$), for a total duration of 50 min (20 min before coapplication with CCh for 30 min) as shown in Figure 5C (open circles), blocked the induction itself of CCh-LTD at both EC- and SC-CA2 synapses with fEPSPs not differing significantly from their respective baseline levels (Fig. 5C, EC-CA2, red open circles, 30 min into CCh: Wilcoxon test, $p = 0.8125$; SC-CA2, blue open circles, 30 min into CCh: Wilcoxon test, $p = 0.4375$). This blockade of CCh-LTD in the presence of 4-DAMP was also significantly different compared

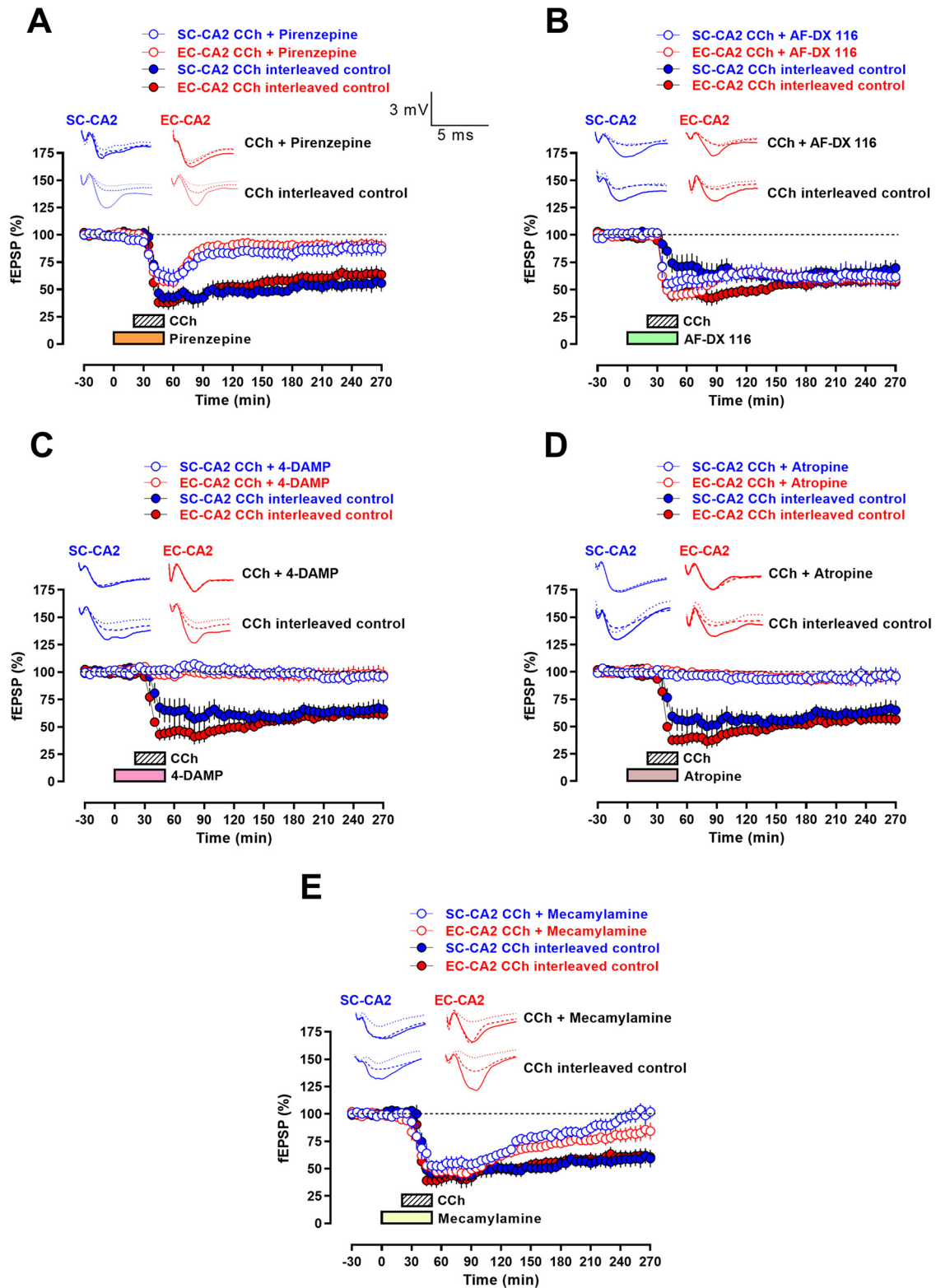


Figure 5. mAChR and nAChR activation plays varied roles in the induction, early, and late phases of CCh-LTD at EC-CA2 and SC-CA2 synapses. **A**, Bath application of the muscarinic M1 receptor antagonist, pirenzepine ($0.5 \mu\text{M}$; 20 min before CCh and 30 min coapplication with CCh), significantly attenuates the early phase as well as the persistent expression of CCh-LTD at both EC- and SC-CA2 synapses (open circles, $n = 9$) compared with CCh-LTD in interleaved control experiments without pirenzepine (filled circles, $n = 8$). **B**, Muscarinic M2 receptor antagonist, AF-DX 116 ($2 \mu\text{M}$) does not block CCh-LTD, and a significant depression persists into the late phase at EC- and SC-CA2 synapses ($n = 7$) at levels comparable to CCh-LTD in interleaved control experiments ($n = 8$). **C**, Muscarinic M3 receptor antagonist, 4-DAMP ($1 \mu\text{M}$), results in the complete abrogation of CCh-LTD at EC- and SC-CA2 synapses ($n = 7$) compared with persistent CCh-LTD in interleaved control experiments ($n = 8$). **D**, The nonselective muscarinic receptor antagonist, atropine ($1 \mu\text{M}$), also results in the complete blockade of CCh-LTD at both EC- and SC-CA2 synapses ($n = 7$) compared with persistent CCh-LTD in interleaved control experiments ($n = 8$). **E**, The nonselective nicotinic receptor antagonist, mecamylamine ($20 \mu\text{M}$), attenuates the late maintenance of CCh-LTD at EC- and SC-CA2 synapses ($n = 7$), while interleaved control experiments ($n = 8$) display significant CCh-induced synaptic depression persisting into the late phase. Data are mean \pm SEM. Analog traces are representative EC-CA2 (red) and SC-CA2 (blue) fEPSPs within 30 min before CCh application (closed line), at 60 min into CCh application (dotted line), and at

with the early and late phases of CCh-LTD in interleaved control experiments without 4-DAMP (Fig. 5C, filled circles) at EC-CA2 (Fig. 5C, 60 min into CCh: U test, $p = 0.0003$; 250 min into CCh: U test, $p = 0.0022$) and SC-CA2 synapses (Fig. 5C, 60 min into CCh: U test, $p = 0.0022$; 250 min into CCh: U test, $p = 0.0289$). A complete blockade of muscarinic receptors with the nonselective muscarinic receptor antagonist, atropine ($1 \mu\text{M}$), bath-applied for a total duration of 50 min (20 min before coapplication with CCh for 30 min) (Fig. 5D, open circles), also resulted in the induction of CCh-LTD being fully abolished, with fEPSPs at EC- and SC-CA2 synapses not significantly different from their respective baseline levels (Fig. 5D, EC-CA2, red open circles, 30 min into CCh: Wilcoxon test, $p = 0.4375$; SC-CA2, blue open circles, 30 min into CCh: Wilcoxon test, $p = 0.3125$). The blockade of CCh-LTD in the presence of atropine was also significantly different compared with the early and late phases of CCh-LTD in interleaved control experiments without atropine (Fig. 5D, filled circles) at EC-CA2 (Fig. 5D, 60 min into CCh: U test, $p = 0.0003$; 250 min into CCh: U test, $p = 0.0003$) and SC-CA2 synapses (Fig. 5D, 60 min into CCh: U test, $p = 0.0140$; 250 min into CCh: U test, $p = 0.0289$). In contrast, application of the nonselective nicotinic receptor antagonist, mecamylamine ($20 \mu\text{M}$), for 50 min (20 min before coapplication with CCh for 30 min) resulted in fEPSPs gradually returning to levels not significantly different from their respective baseline values only by 235 min into CCh application at EC-CA2 synapses (Fig. 5E, EC-CA2, red open circles, 255 min: Wilcoxon test, $p = 0.0781$) and by 190 min into CCh application at SC-CA2 synapses (Fig. 5E, SC-CA2, blue open circles, 210 min: Wilcoxon test, $p = 0.0781$). At both EC- and SC-CA2 synapses, the early phase of CCh-LTD was not significantly different in the presence of mecamylamine compared with its interleaved control (Fig. 5E, filled circles) experiments without mecamylamine (Fig. 5E, EC-CA2, 60 min into CCh: U test, $p = 0.6794$; SC-CA2, 60 min into CCh: U test, $p = 0.1514$), suggesting that nicotinic receptors do not play a significant role in mediating the early phase of CCh-LTD at CA2 synapses. An inspection of the fEPSP (%) values at SC-CA2 in Figure 5E by the end of the recording period (250 min into CCh application) for experiments with mecamylamine reveals that the SC-CA2 fEPSPs attained a mean value of $101.8 \pm 6.078\%$ and were not significantly different compared with its baseline levels (Fig. 5E, SC-CA2, blue open circles, 270 min: Wilcoxon test, $p > 0.9999$). The SC-CA2 fEPSPs at this time point, for experiments with mecamylamine, were also significantly different compared with the late phase of CCh-LTD in its interleaved control experiments without mecamylamine (Fig. 5E, SC-CA2, 250 min into CCh: U test, $p = 0.0037$). By the end of the recording period (250 min into CCh application) for experiments with mecamylamine in Figure 5E, the EC-CA2 fEPSPs attained a mean value of $84.41 \pm 7.896\%$ and were not significantly different compared with its baseline levels (Fig. 5E, EC-CA2, red open circles, 270 min: Wilcoxon test, $p = 0.1094$). However, this attenuation of fEPSPs at EC-CA2 in the presence of mecamylamine was not significantly different compared against the late phase of CCh-LTD in its interleaved control experiments without mecamylamine (Fig. 5E, EC-CA2, 250 min into CCh: U test, $p = 0.0541$). Together, the inspection of fEPSP (%) values by the end of the recording period for experiments with mecamylamine in Figure 5E and their

comparison against baseline values as well as against CCh-LTD in interleaved control experiments separately, suggest that, although mecamylamine does attenuate the late persistence of CCh-LTD at both EC-CA2 and SC-CA2 synapses, it does not fully abrogate the synaptic depression at EC-CA2, as opposed to SC-CA2 synapses where mecamylamine appears to nearly eliminate the late phase of CCh-LTD by the end of the recording period.

The results presented in Figure 5A, C, E are indicative of a strong dependency for muscarinic M3 receptor activation in the early facilitation of CCh-LTD at CA2 synapses with a weaker role for muscarinic M1 receptors, and suggest that activation of nicotinic receptors plays a role in the late maintenance of CCh-LTD. The observed role for nicotinic receptors is in contrast to the recent study in mice where nicotinic receptors were not observed to be involved in CCh-induced synaptic depression in CA2 neurons (Robert et al., 2020). However, we suspect that the aforementioned study could not detect a role for nicotinic receptors in CCh-LTD because of a short recording period. Similar to their results, we also observed that the acute depression following CCh application was not blocked by the nicotinic antagonist. Together, the data presented in Figure 5A–E suggest that, while activation of muscarinic M3 and M1 ACh receptors, and nicotinic ACh receptors, facilitates CCh-LTD, albeit with differences in their contribution to the induction, early, and late phases of CCh-LTD, the induction itself of CCh-LTD at CA2 synapses is mediated through muscarinic and not nicotinic receptor activation. While these results are presented, it is also noted that more confidence in the role of the different muscarinic receptors in mediating CCh-LTD could only be derived by even more selective and targeted receptor blockade given that pharmacological agents, such as pirenzepine used in this study, show moderate cross-selectivity to other muscarinic receptor subtypes as well (Marino et al., 1998). Nonetheless, the effects observed in this study do suggest varied roles of the different cholinergic receptors in mediating CCh-LTD at CA2 synapses.

Prior synaptic depression mediated by cholinergic receptor activation primes CA2 synapses for LTP

As the maintenance of CCh-induced synaptic depression at CA2 synapses was shown to be protein synthesis-dependent, we explored whether such protein synthesis and/or other activated signaling downstream of cholinergic receptor activation could alter the state of CA2 synapses to regulate subsequently induced synaptic plasticity. We hypothesized that, if there is a common pool of plasticity-related proteins between LTD and LTP, then this could potentially “prime” the depressed synapses for LTP as well when stimulus strength is altered. To this end, we performed single-pathway experiments wherein we stimulated the EC inputs alone to CA2 at the SLM and recorded fEPSPs from the CA2 dendritic region. In the absence of CCh priming, a weak tetanization (WTET) delivered at EC-CA2 synapses normally results only in a short-lasting synaptic potentiation called early LTP (E-LTP) that decays to baseline levels by 95 min after WTET (Fig. 6A, red circles, 95 min: Wilcoxon test, $p = 0.1094$). Next, we explored how CCh priming affects WTET-induced LTP at EC-CA2 synapses. Upon recording a 30 min stable baseline, CCh was bath-applied for 30 min, which resulted in a significant synaptic depression at the EC-CA2 synapses (Fig. 6B, red circles, 60 min: Wilcoxon test, $p = 0.0078$). However, after 60 min into CCh application, the stimulus strength of the EC input was increased such that the fEPSPs returned to values comparable to the initial average baseline values before CCh application (Fig. 6B, red circles, 80 min: U test, $p = 0.1949$). As shown in Figure 6B, a

←

250 min into CCh application (hatched line). Top, Analog traces in the presence of specific receptor antagonists. Bottom, Analog traces for its respective interleaved control experiments. Calibration: A–E, 3 mV, 5 ms.

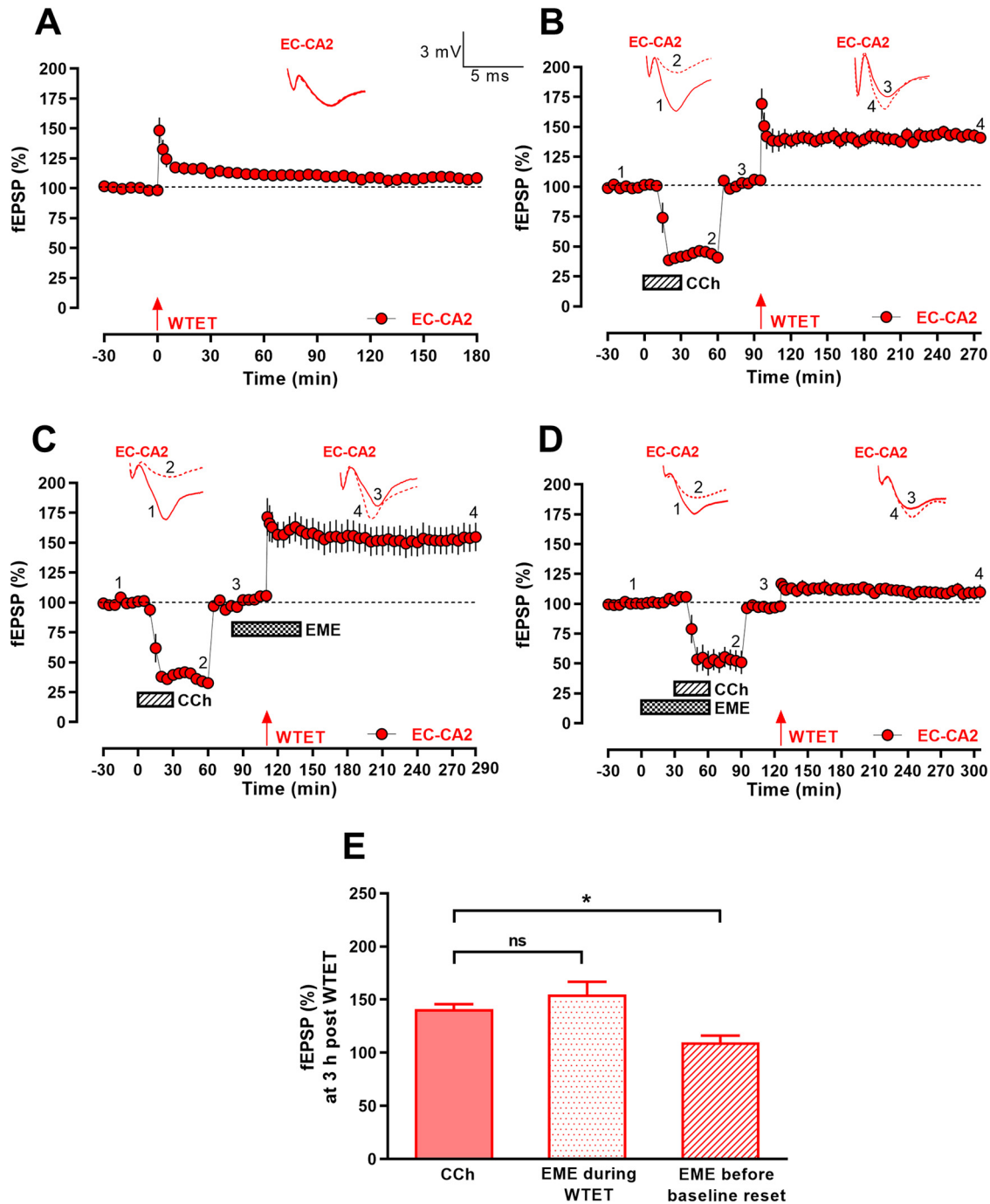


Figure 6. Prior synaptic depression by cholinergic receptor activation primes EC-CA2 synapses for persistent LTP expression in response to WTET delivered at a later point in time. **A**, Control single-pathway experiment where EC fibers alone to CA2 were stimulated without prior CCh priming and WTET delivered at EC-CA2 following a stable baseline of 30 min, resulted in a short-lasting potentiation (E-LTP) ($n = 8$). **B**, Persistent potentiation (L-LTP) results when WTET was induced at EC-CA2 following a new reset stable baseline of 30 min on increasing the stimulus strength 1 h into CCh application ($n = 8$). **C**, Late inhibition of protein synthesis by bath application of the protein synthesis inhibitor, emetine (EME; $20 \mu\text{M}$), during the delivery of WTET at EC-CA2 does not abrogate CCh-primed reinforcement of WTET-induced LTP such that persistent LTP is still observed ($n = 9$). **D**, Early inhibition of protein synthesis during CCh-LTD with emetine bath-applied 30 min before CCh and 30 min together with CCh prevents the reinforcement of WTET-induced LTP at EC-CA2 ($n = 7$). **E**, Summary bar chart comparing fEPSP (%) 3 h after WTET at EC-CA2 from **B** (CCh) against **C** (EME during WTET) and **D** (EME before baseline reset). Differences between groups: * $p < 0.05$; ns, not significant, $p > 0.05$; Dunn's multiple comparisons *post hoc* analysis following Kruskal–Wallis test. Data are mean \pm SEM. **B–D**, Analog traces are representative EC-CA2 (red) fEPSPs within 30 min before CCh application (dashed line 1), at 60 min into CCh application (hatched line 2), within 30 min before WTET (dashed line 3), and at 180 min after WTET (hatched line 4). **A**, Analog traces are representative EC-CA2 fEPSPs within the 30 min baseline before WTET (dashed line) and at 180 min after WTET (hatched line). Calibration: **A–D**, 3 mV, 5 ms.

new stable baseline was thereafter recorded at the increased stimulus strength for another 30 min, following which WTET was delivered to the EC-CA2 pathway. We observed that priming from CCh-LTD results in the transformation of a transient WTET-induced E-LTP to a long-lasting late LTP (L-LTP) at EC-CA2

maintained for 3 h after WTET (Fig. 6B, red circles, 275 min: Wilcoxon test, $p = 0.0078$). Thus, CCh-LTD serves as a metaplastic trigger for the reinforcement of subsequently induced LTP by stimuli subthreshold for producing L-LTP at EC-CA2 synapses. Moreover, the magnitude of synaptic potentiation at EC-CA2 in

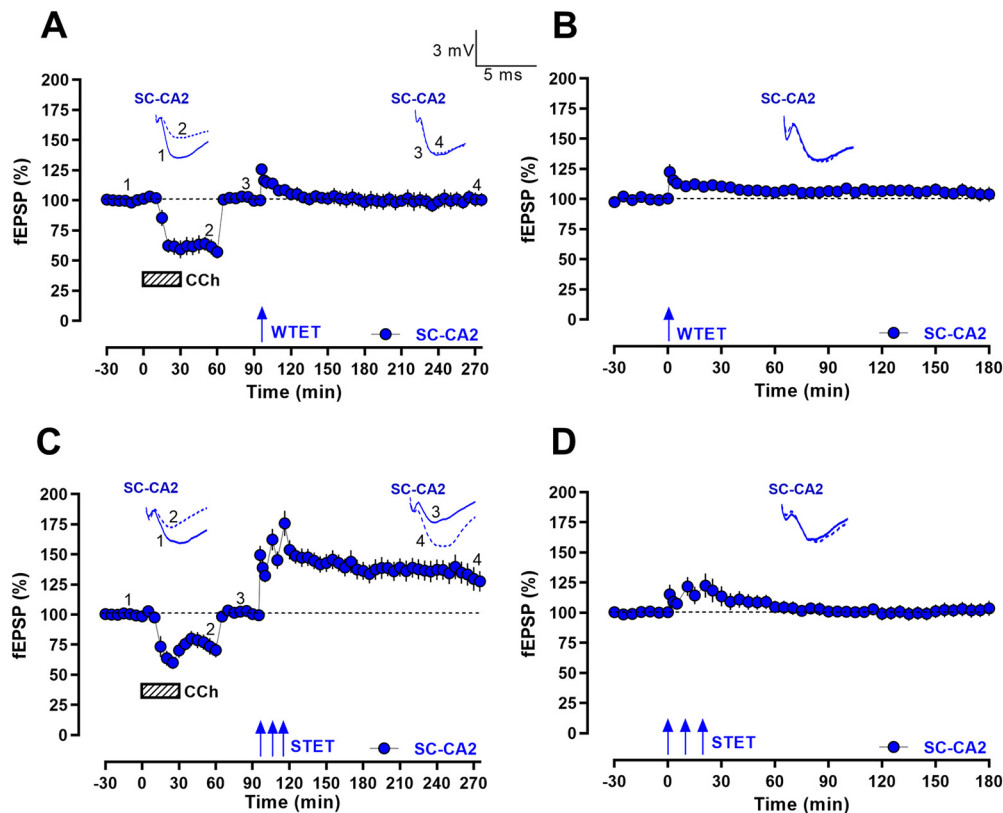


Figure 7. LTP is expressed at SC-CA2 synapses in response to STET but not WTET subsequent to CCh-LTD. **A**, In single-pathway experiments where SC fibers to CA2 alone were stimulated, WTET delivered following a new reset stable 30 min baseline on increasing stimulus strength 1 h into CCh application, elicited only a transient potentiation that quickly decayed to baseline levels ($n = 8$). **B**, In the control experiment without prior CCh priming, WTET delivered at SC-CA2 following a stable 30 min baseline also results in a transient potentiation that quickly decays to baseline levels ($n = 6$). **C**, Strong tetanic stimulation (STET) following CCh-LTD elicits LTP expression at SC-CA2. STET delivered at SC-CA2 following the new reset 30 min baseline on increasing the stimulus strength 1 h into CCh application led to the expression of persistent synaptic potentiation (LTP) up to 3 h ($n = 13$). **D**, Control experiment without prior CCh priming, where STET was delivered at SC-CA2 following a stable baseline of 30 min, resulted in only a transient potentiation that quickly decayed to baseline levels ($n = 10$). Data are mean \pm SEM. **A**, **C**, Analog traces are representative SC-CA2 (blue) fEPSPs within 30 min before CCh application (closed line 1), at 60 min into CCh application (hatched line 2), within 30 min before TET (closed line 3), and at 180 min after TET (hatched line 4). **B**, **D**, Analog traces are representative SC-CA2 fEPSPs within the 30 min baseline before TET (closed line) and at 180 min after TET (hatched line). Calibration: **A–D**, 3 mV, 5 ms.

the early phase of LTP following CCh priming in Figure 6B was observed to be significantly greater compared with that without CCh priming in Figure 6A (60 min after WTET: U test, $p = 0.0002$). LTP being a temporal phase of LTP that supplants E-LTP over time (Sweatt, 2010), these results further suggest that priming by CCh-LTD reinforces WTET-induced LTP at EC-CA2 synapses by increasing the magnitude of E-LTP as well as facilitating the expression of LTP.

In order to understand whether this “primed” reinforcement of LTP is protein synthesis-dependent, we bath-applied the protein synthesis inhibitor, emetine, 15 min into resetting the baseline by increasing the EC input stimulus strength after 60 min into CCh application (Fig. 6C). As shown in Figure 6C, after recording a new stable baseline for 15 min at the increased stimulus strength, emetine was bath-applied for a total duration of 60 min, and WTET was delivered to EC-CA2 30 min into emetine application. However, a significant synaptic potentiation was still observed at EC-CA2 3 h after WTET (Fig. 6C, red circles, 290 min: Wilcoxon test, $p = 0.0039$). This prompted us to explore whether early protein synthesis inhibition during CCh-LTD could affect the primed LTP. Interestingly, when emetine was applied for a total duration of 60 min (30 min before and 30 min coapplication with CCh) as shown in Figure 6D, the EC-CA2 synaptic potentials returned to levels not significantly different from the reset baseline potentials by 95 min after

WTET (Fig. 6D, red circles, 220 min: Wilcoxon test, $p = 0.0781$). Although there is a small yet significant post-tetanic potentiation at EC-CA2 following WTET in Figure 6D (red circles, 1 min after WTET: Wilcoxon test, $p = 0.0156$), it is significantly attenuated compared with the post-tetanic potentiation in Figure 6B (1 min after WTET: U test, $p = 0.0006$). These data demonstrate that protein synthesis initiated in response to CCh-induced synaptic depression is critical for the early induction phase as well as the enabling of LTP expression on a sequential increase in stimulus strength followed by WTET at EC-CA2. Figure 6E (bar chart) represents EC-CA2 fEPSP (%) at 3 h after WTET from Figure 6B compared against Figure 6C and Figure 6D, summarizing the effect of protein synthesis inhibition at different time points on the persistence of CCh-primed LTP at EC-CA2 synapses.

Similar to the LTP reinforcement observed at EC-CA2 synapses that were weakly stimulated subsequent to CCh-LTD, we next explored whether this metaplastic effect is also displayed by the SC-CA2 synapses. We designed a single-pathway experiment with a timeline similar to that in Figure 6B, with the exception that, in place of EC stimulation, the SC-CA2 pathway was stimulated at the proximal SR and fEPSPs were recorded from the CA2 dendritic region (Fig. 7A). After 30 min of an initial stable baseline, CCh was bath-applied for 30 min, which resulted in a significant synaptic depression at SC-CA2 (Fig. 7A, SC-CA2, blue circles, 60 min: Wilcoxon test, $p = 0.0078$). Sixty minutes

into CCh application, the input stimulus strength for SC-CA2 was increased such that its fEPSPs returned to values comparable to the initial average baseline values before CCh application (Fig. 7A, SC-CA2, blue circles, 80 min: U test, $p = 0.2786$). After recording a new reset stable baseline for 30 min at the increased stimulus strength, WTET was delivered to the SC-CA2 pathway. However, unlike the EC-CA2 pathway, the SC-CA2 synapses did not display a persistent LTP and fEPSPs decayed to the reset baseline potentials by 15 min after WTET (Fig. 7A, SC-CA2, blue circles, 110 min: Wilcoxon test, $p = 0.5469$). Figure 7B shows the control single-pathway experiment without CCh priming where a WTET delivered at SC-CA2 following a 30 min stable baseline recording results in a transient potentiation that decays to baseline levels by 15 min after WTET (Fig. 7B, SC-CA2, blue circles, 15 min: Wilcoxon test, $p = 0.0938$). As SC-CA2 synapses are different from EC-CA2 in their plasticity expression and have been shown in multiple previous studies to be resistant to canonical activity-dependent LTP (Zhao et al., 2007; Chevalleyre and Siegelbaum, 2010; Dasgupta et al., 2017), we were intrigued to explore whether a stronger stimulus could facilitate LTP reinforcement after CCh priming in the SC-CA2 pathway. To test this possibility, a strong tetanization (STET) consisting of three trains of high-frequency stimulation at 100 Hz was delivered at SC-CA2 following CCh priming (Fig. 7C). Similar to the experiment timeline in Figure 7A, after 30 min of an initial stable baseline, CCh was bath-applied for 30 min, which resulted in a significant synaptic depression at SC-CA2 (Fig. 7C, SC-CA2, blue circles, 60 min: Wilcoxon test, $p = 0.0005$). Sixty minutes into CCh application, the input stimulus strength for SC-CA2 was increased to revert fEPSPs to values comparable to the initial average baseline values before CCh application (Fig. 7C, SC-CA2, blue circles, 80 min: U test, $p = 0.3358$). Following a new stable baseline of 30 min, STET was delivered to the SC-CA2 pathway, which resulted in persistent LTP that remained significantly higher than its reset baseline potentials for 3 h (Fig. 7C, SC-CA2, blue circles, 275 min: Wilcoxon test, $p = 0.0398$). Figure 7D shows the single-pathway control recording where SC-CA2 synapses were subjected to STET following a 30 min stable baseline recording, resulting in only a transient potentiation that quickly decayed to baseline levels by 15 min after STET (Fig. 7D, SC-CA2, blue circles, 15 min: Wilcoxon test, $p = 0.2754$). Thus, cholinergic receptor activation-induced synaptic depression primes both EC and SC synapses onto CA2 for persistent LTP, albeit in response to different strength of plasticity-inducing tetanic stimuli.

CCh-primed LTP reinforcement at cortical synaptic inputs to CA2 coexists with concurrent and sustained CCh-LTD in the SC pathway

The spatial segregation of incoming information via the SC and EC pathways converging onto CA2 proximal and distal dendritic regions, respectively, raises the possibility of a heterosynaptic trans-compartmental interaction in the processing of incoming synaptic inputs to CA2 neurons. With the existence of a primed LTP at EC-CA2 synapses demonstrated in response to prior cholinergic activation-induced synaptic depression in single-pathway experiments (Fig. 6B), we were thus intrigued to perform two-pathway experiments with similar experimental design to explore whether there is an interaction between the EC and SC pathways modulating the expression of the observed LTP. To determine this, we performed experiments wherein we stimulated both EC and SC fibers onto CA2 but differentially changed the stimulus strength of both pathways after CCh-induced synaptic depression. First, we performed a two-pathway experiment

involving stimulation of EC and SC fibers, wherein a stable baseline was recorded for 30 min, following which CCh was bath-applied for 30 min, which resulted in a significant synaptic depression at EC (Fig. 8A, red circles, 60 min: Wilcoxon test, $p = 0.0156$) and SC (Fig. 8A, blue circles, 60 min: Wilcoxon test, $p = 0.0156$) inputs to CA2. After 60 min into CCh application, the stimulus strength of EC inputs alone was increased such that fEPSPs at EC-CA2 reverted to values comparable to its initial average baseline values before CCh application (Fig. 8A, EC-CA2, red circles, 80 min: U test, $p = 0.7104$). Stimulus strength for the SC-CA2 pathway was unaltered such that SC-CA2 synapses displayed significant and sustained CCh-LTD until the end of the recording period (Fig. 8A, SC-CA2, blue circles, 275 min: Wilcoxon test, $p = 0.0156$). In the EC-CA2 pathway, however, after 30 min of a stable reset baseline, WTET was delivered, which resulted in persistent LTP lasting 3 h (Fig. 8A, EC-CA2, red circles, 275 min: Wilcoxon test, $p = 0.0156$). Figure 8B shows the control two-pathway experiment without CCh priming, where WTET is delivered to EC-CA2 following a 30 min stable baseline recording, resulting in only a short-lasting E-LTP that decays to baseline levels by 40 min after WTET (Fig. 8B, EC-CA2, red circles, 40 min: Wilcoxon test, $p = 0.0781$). SC-CA2 synapses are subjected to baseline stimulation throughout and display stable synaptic responses until the end of the recording period (Fig. 8B, SC-CA2, blue circles, 180 min: Wilcoxon test, $p = 0.9375$). As shown in Figure 8C, we also compared changes in the presynaptic release probability by performing paired-pulse stimulation at EC-CA2 synapses at three different points in the experiment timeline (before CCh application, at a time point in the reset baseline after CCh application, and after 30 min after WTET), for two-pathway experiments performed from Figure 8A. Pairs of stimulation pulses with an interstimulus interval of 10, 30, 50, 70, 100, 150, and 250 ms were delivered at EC-CA2 at a point during baseline recording before CCh application (pre CCh), at a point during the new reset baseline taken after increasing stimulus strength at EC (post CCh baseline reset) and after 30 min after WTET (post WTET). However, the paired-pulse ratios at EC-CA2 between the three experimental time points were not significantly different from each other (Fig. 8C, Kruskal–Wallis test with Dunn’s multiple comparisons *post hoc* analysis, interstimulus intervals 10 ms: $p = 0.3672$, 30 ms: $p = 0.5367$, 50 ms: $p = 0.1054$, 70 ms: $p = 0.7831$, 100 ms: $p = 0.4154$, 150 ms: $p = 0.2378$, 250 ms: $p = 0.8268$), suggesting that no significant changes in presynaptic release probability are induced at EC-CA2 synapses between the three experimental time points assessed. Figure 8D shows the percent paired-pulse ratio normalized by the average pre CCh paired-pulse ratio for the paired-pulse stimulation experiments at 10 ms interstimulus interval from Figure 8C. Although there is a slight increase, at 10 ms interstimulus interval, between the normalized EC-CA2 paired-pulse ratio before CCh application (pre CCh) and at a point in the new reset baseline after increasing EC stimulus strength (post CCh baseline reset), it is not statistically significant (Fig. 8D, Kruskal–Wallis test, $p = 0.3672$, followed by Dunn’s multiple comparisons *post hoc* analysis, $p = 0.4550$). Similarly, the normalized EC-CA2 paired-pulse ratio at a point in the new reset baseline (post CCh baseline reset) and after 30 min after WTET (post WTET) are not significantly different from each other (Fig. 8D, Kruskal–Wallis test, $p = 0.3672$, followed by Dunn’s multiple comparisons *post hoc* analysis, $p > 0.9999$), suggesting that the observed CCh-primed LTP at EC-CA2 in the two-pathway experiment is not associated with a significant change in the presynaptic glutamate release probability after 30 min after WTET.

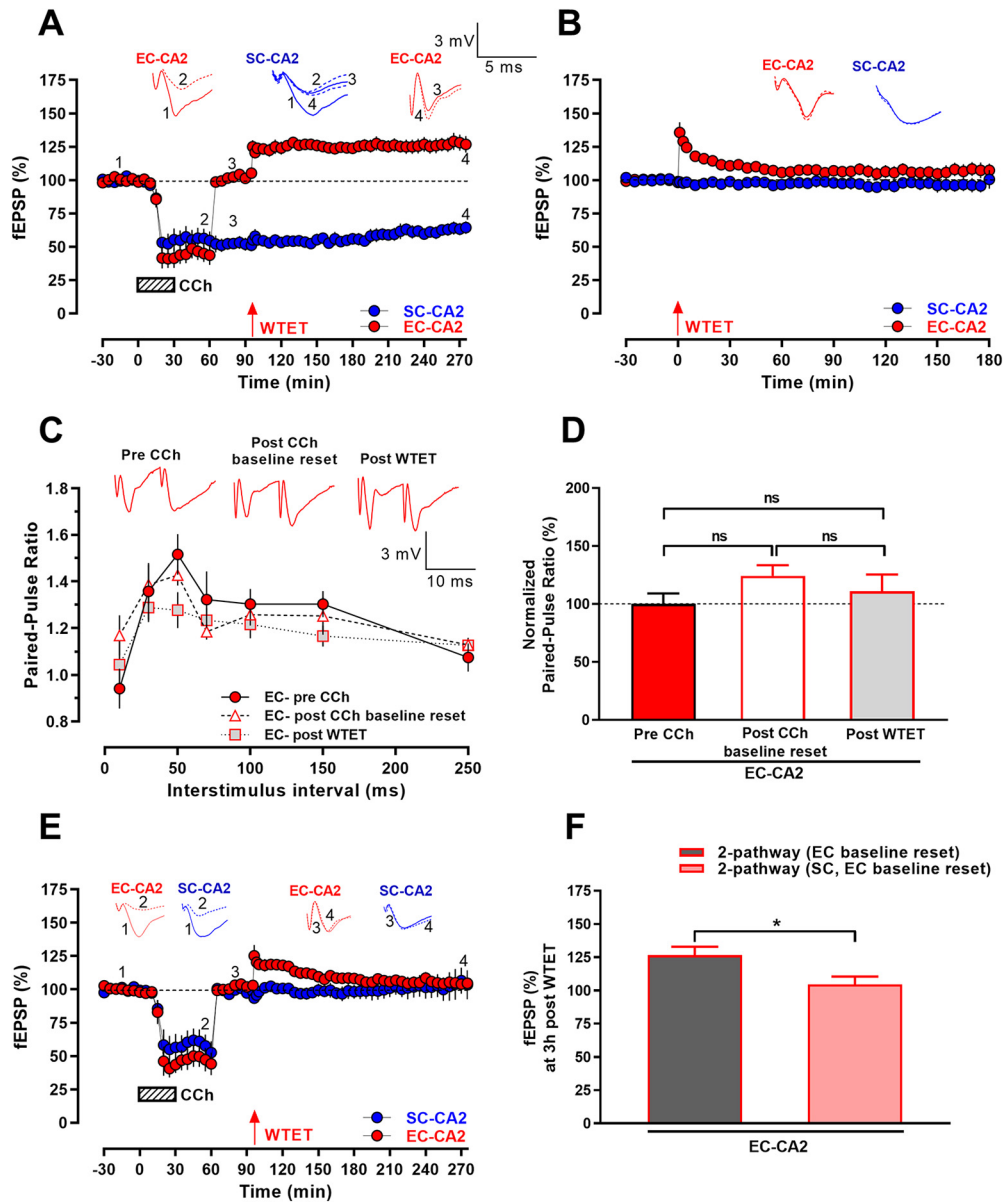


Figure 8. CCh-primed LTP reinforcement at EC-CA2 steadily coexists with concurrent CCh-LTD at SC-CA2 synapses. **A**, In two-pathway experiments where EC and SC fibers to CA2 were stimulated, WTET delivered at EC-CA2 following a reset stable baseline on increasing the stimulus strength at EC-CA2 alone 1 h into CCh application, results in the persistent expression of LTP at EC-CA2, that coexists with sustained CCh-LTD at SC-CA2 ($n = 7$). **B**, Control experiment without prior CCh priming results in only a short-lasting potentiation on delivery of WTET at EC-CA2 ($n = 7$). **C**, No significant differences were observed for paired-pulse ratios at EC-CA2 analyzed for the experiments in **A**, at three stages during the recording: In the baseline before CCh application (pre CCh), in the reset baseline after increasing stimulus strength at EC-CA2 (post CCh baseline reset), and 30 min after WTET at EC-CA2 (post WTET) ($n = 6$). **D**, EC-CA2 paired-pulse ratios at 10 ms interstimulus interval from **C** normalized by the average Pre CCh paired-pulse ratio and compared among the three stages (Dunn's multiple comparisons *post hoc* analysis following Kruskal–Wallis test, ns, not significant, $p > 0.05$). **E**, Increasing the stimulus strength at SC-CA2 along with EC-CA2 following CCh priming prevents LTP reinforcement at EC-CA2 subsequently subjected to WTET such that only a short-lasting potentiation ensues at EC-CA2 ($n = 6$). **F**, Summary bar chart comparing fEPSP (%) at EC-CA2 3 h after WTET between **A** (two-pathway [EC baseline reset]) and **E** (two-pathway [SC, EC baseline reset]) (U test, $*p < 0.05$). Data are mean \pm SEM. **A**, **E**, Analog traces are representative EC-CA2 (red) and SC-CA2 (blue) fEPSPs within 30 min before CCh application (dashed line 1), at 60 min into CCh application (hatched line 2), within 30 min before WTET at EC-CA2 (closed line 3), and at 180 min after WTET at EC-CA2 (hatched line 4). **B**, Analog traces are representative EC-CA2 and SC-CA2 fEPSPs within the 30 min baseline before WTET at EC-CA2 (closed line) and at 180 min after WTET at EC-CA2 (hatched line). **C**, Analog traces are representative EC-CA2 (red) fEPSPs for the paired-pulse stimulation at 10 ms interstimulus interval. Calibration: **A**, **B**, **E**, 3 mV, 5 ms; **C**, 3 mV, 10 ms.

In a separate two-pathway experiment, we followed the same experimental design as Figure 8A, with the exception that the stimulus strength was increased after 60 min into CCh application at SC-CA2 in addition to the EC-CA2 pathway (Fig. 8E). After a 30 min stable baseline, CCh was bath-applied for 30 min, which resulted in a significant synaptic depression at both EC (Fig. 8E, red circles, 60 min: Wilcoxon test, $p = 0.0313$) and SC inputs to CA2 (Fig. 8E, blue circles, 60 min: Wilcoxon test, $p = 0.0313$). After 60 min into CCh application, stimulus strength

at both SC and EC pathways was increased such that synaptic potentials at both pathways reverted to values comparable to the initial average baseline values before CCh application (Fig. 8E, EC-CA2, red circles, 80 min: U test, $p = 0.1320$; SC-CA2, blue circles, 80 min: U test, $p > 0.9999$). Thirty minutes following the reset stable baseline at EC-CA2 and SC-CA2, WTET was delivered at the EC-CA2 pathway alone (Fig. 8E). Unlike Figure 8A, this did not result in the late persistence of LTP at EC-CA2 with fEPSPs at EC-CA2 decaying to baseline levels by 35 min

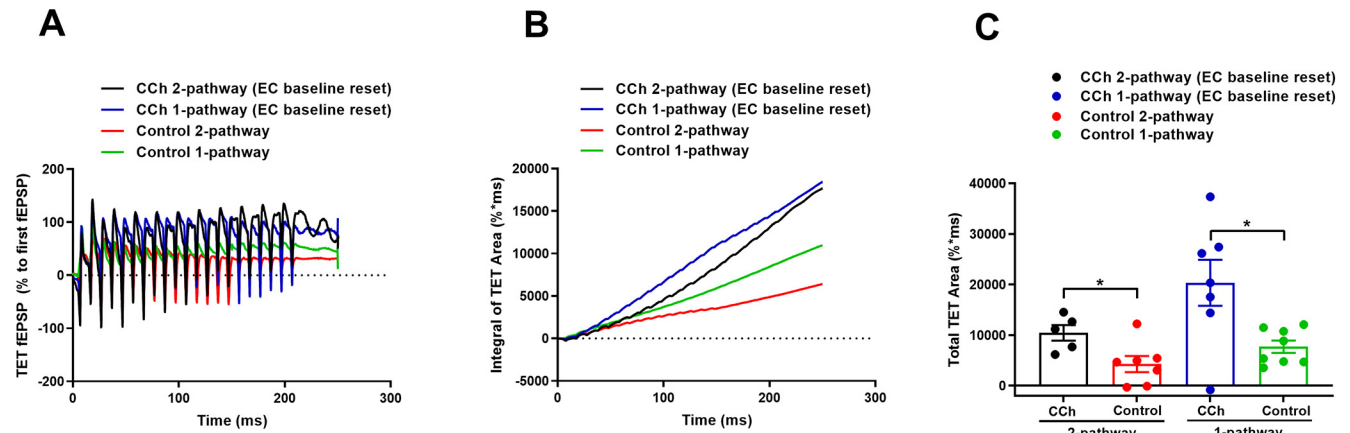


Figure 9. Comparison of the effect of CCh priming on tetanic stimuli-mediated summation of fEPSPs at EC-CA2 synapses. **A**, Average field potential traces in response to 100 Hz/s from single ($n = 8$; green line) and two-pathway ($n = 7$; red line) EC-CA2 WTET control experiments without CCh priming (from Figs. 6A and 8B, respectively), and from single ($n = 7$; blue line) and two-pathway ($n = 5$; black line) experiments with CCh-induced synaptic depression before WTET at EC-CA2 (from Figs. 6B and 8A, respectively). The field potential traces were normalized to the amplitude of the first fEPSP in the train of high-frequency tetanic stimuli, and artifacts were truncated by linear interpolation. **B**, Integral of normalized TET area at EC-CA2 of experiments conducted with and without CCh priming. **C**, Comparison of the total normalized TET area of individual experiments, with and without CCh priming. Total normalized TET area at EC-CA2 after CCh priming in single and two-pathway experiments is significantly greater compared with their respective control experiments without CCh priming. Data show individual data points; mean \pm SEM. Significant differences between the two groups: $*p < 0.05$ (U test).

after WTET (Fig. 8E, EC-CA2, red circles, 130 min: Wilcoxon test, $p = 0.0625$). The fEPSPs at SC-CA2 were not significantly different from its reset baseline levels until the end of the recording period (Fig. 8E, SC-CA2, blue circles, 275 min: Wilcoxon test, $p = 0.6875$). Figure 8F (bar chart) demonstrates significant attenuation of the net EC-CA2 fEPSP (%) at 3 h after WTET in Figure 8E compared against Figure 8A (U test, $p = 0.0350$). Thus, the persistence of LTP at EC-CA2 following CCh-induced synaptic depression is influenced by the strength of concurrent synaptic responses at SC-CA2 and coexists with sustained CCh-LTD in the SC-CA2 pathway. EC-CA2 postsynaptic potentials 3 h following WTET were also not significantly different between the two-pathway experiment in Figure 8A and the single-pathway EC-CA2 experiment in Figure 6B (EC-CA2, 3 h after WTET: U test, $p = 0.0939$). However, the net post-tetanic potentiation immediately following WTET was significantly higher in the single-pathway EC-CA2 experiments in Figure 6B compared with the two-pathway experiments performed in Figure 8A (EC-CA2, 1 min after WTET: U test, $p = 0.0059$) and Figure 8E (EC-CA2, 1 min after WTET: U test, $p = 0.0127$). It is unlikely that the observed reduction in the magnitude of net post-tetanic potentiation is because of the afferent stimulation of both pathways, as we observed comparable levels of net post-tetanic potentiation at EC-CA2 in the control single-pathway (Fig. 6A) and two-pathway (Fig. 8B) EC-CA2 WTET experiments without CCh priming (EC-CA2, 1 min after WTET: U test, $p = 0.6126$). We speculate that synaptic stimulation of SC-CA2 on CCh priming interferes with the expression of post-tetanic potentiation at EC-CA2 in the two-pathway experiment contributing to the observed scaling down of post-tetanic potentiation, although the mechanisms mediating this heterosynaptic effect remain to be determined.

Further, to understand how prior synaptic depression induced by cholinergic receptor activation may alter the level of depolarization in CA2 neurons in response to subsequent delivery of WTET at EC-CA2 compared with control experiments where WTET was delivered at EC-CA2 in the absence of cholinergic activation, we analyzed and compared the tetanic stimuli-mediated summation of field potentials at EC-CA2 with and without CCh priming (Fig. 9A–C). Figure 9A shows the average EC-CA2 field potential traces

in response to 100 Hz/s from single (Fig. 6A) and two-pathway (Fig. 8B) EC-CA2 WTET control experiments without CCh priming, and from single (Fig. 6B) and two-pathway (Fig. 8A) experiments where cholinergic receptor activation was induced with CCh application before WTET at EC-CA2. The field potential traces were normalized to the amplitude of the first fEPSP in the train of high-frequency tetanic stimuli. Figure 9B depicts the integral of normalized tetanization (TET) area at EC-CA2 of single and two-pathway experiments conducted with and without CCh priming. A comparison of the total normalized TET area at EC-CA2 with and without CCh priming, as depicted in Figure 9C, shows that there is a significant increase in the total normalized TET area at EC-CA2 after CCh priming in both single pathway (Fig. 9C, U test, $p = 0.0205$), and two-pathway experiments (Fig. 9C, U test, $p = 0.0177$) compared with their respective control experiments without CCh priming. This suggests that the priming effect by prior CCh-induced synaptic depression significantly increases the level of depolarization in CA2 neurons immediately in response to WTET at EC-CA2. This observed increase in TET area after CCh priming is also suggestive of a possible enhancement of transmitter release during tetanic stimulation in the CCh-primed experiments compared with control experiments without CCh priming, which may be partly contributing to the early phase of CCh-primed LTP at EC-CA2 observed in Figures 6B and 8A. However, we noted from the paired-pulse stimulation experiments in Figure 8C that, by 30 min into LTP induction, there is no significant presynaptic component in the reinforcement of LTP as observed by comparable levels of paired-pulse ratios before and after tetanic stimulation at EC-CA2 in the two-pathway experiment. Overall, our data demonstrate a cooperative interaction between concurrent CCh-induced LTD at SC-CA2 and the metaplastic reinforcement of LTP at EC-CA2 synapses. Interestingly, the CCh-primed LTP at EC-CA2 synapses is downscaled by reversing the synaptic weights at SC-CA2 after CCh priming to baseline levels.

Discussion

Cholinergic modulation of neuronal activity is critical to learning and memory processes in multiple neural systems (Gold, 2003;

Hasselmo, 2006). Numerous studies deciphered the role of cholinergic signaling in the hippocampus for memory formation, particularly episodic and spatial memory, and synaptic plasticity, including LTP and LTD (Teles-Grilo Ruivo and Mellor, 2013; Haam and Yakel, 2017). While cholinergic receptor activation-mediated synaptic depression has been reported in multiple brain regions, including hippocampal CA1 (Kirkwood et al., 1999), CA3 (Williams and Johnston, 1990), visual cortex (Kirkwood et al., 1999), perirhinal cortex (Massey et al., 2001), and more recently in CA2 neurons (Robert et al., 2020), previous studies have not looked into the role of cholinergic modulation in the bidirectional and temporal regulation of plasticity at CA2 synapses that we have in the present study. The results demonstrate a dynamic modulation of synaptic plasticity in hippocampal area CA2 across time owing to cholinergic receptor activation with the nonselective cholinergic agonist, CCh, that induces a protein synthesis-dependent LTD at both EC- and SC-CA2 synapses. The results further suggest that muscarinic and nicotinic ACh receptors are functionally present in area CA2, mediating different phases of CCh-LTD at EC- and SC-CA2 synapses. It is also notable that the expression mechanisms of CCh-LTD at CA2 synapses resemble LTD induced by activation of Gq-coupled Group I metabotropic glutamate receptors (mGluR-LTD) at CA1 synapses which is also protein synthesis-dependent and NMDAR-independent (Huber et al., 2000, 2001; Volk et al., 2007).

Importantly, the present work demonstrates that prior induction of synaptic depression by cholinergic receptor activation acts as a “priming” signal that subserves the metaplastic reinforcement of synaptic potentiation in CA2 neurons in response to a later bout of subthreshold plasticity-inducing stimuli. Metaplasticity regulates plasticity thresholds based on the history of synaptic activity such that modifications of neural activity at one point in time can alter the ability of synapses to subsequently generate synaptic plasticity, such as LTP or LTD (Abraham, 2008). We show that prior synaptic depression induced by cholinergic receptor activation primes EC-CA2 synapses for persistent LTP expression in response to a later bout of weak tetanizing stimuli which normally elicits only a short-lasting LTP. We therefore propose that metaplasticity triggered by priming activity of CCh-induced synaptic depression shifts the threshold (θ) for conventional STET-induced persistent LTP at EC-CA2 synapses, to a lower threshold (θ') such that WTET can result in the expression of L-LTP, similar to a Bienenstock-Cooper-Munro model-like sliding synaptic modification threshold that depends on the slowly varying time-averaged value of neural activity (Bienenstock et al., 1982; Jedicke, 2002).

We also report that prior CCh-induced synaptic depression allows for the induction and persistent expression of LTP at SC-CA2 synapses in response to strong tetanizing stimuli, which was otherwise ineffective at inducing LTP at SC-CA2. Unlike EC-CA2 synapses, the SC-CA2 pathway displayed only a transient potentiation in response to WTET delivered subsequent to CCh-LTD. This difference among EC- and SC-CA2 synapses in the strength of induction stimuli required for the CCh-primed LTP reinforcement could be because of the inherent differences in plasticity expression along the proximo-distal dendritic axis of CA2 neurons, with the proximal SC-CA2 synapses being resistant to activity-dependent LTP (Carstens and Dudek, 2019). The distinctive resistance to plasticity displayed by SC-CA2 synapses has been attributed to multiple suppressive factors that include the enriched expression of the scaffolding protein, regulator of G

protein signaling 14 in CA2 neurons (S. E. Lee et al., 2010; Evans et al., 2018), higher endogenous calcium buffering, and enhanced calcium extrusion at CA2 dendritic spines (Simons et al., 2009), dense expression of the specialized extracellular matrix structures called perineuronal nets (Carstens et al., 2016), high mitochondrial calcium uptake in CA2 neurons (Farris et al., 2019), and the relatively high expression of Group III metabotropic glutamate receptors in area CA2 (Dasgupta et al., 2020). We conjecture that metaplastic synaptic modifications may significantly contribute to plasticity expression at the CA3→CA2 pathway when studied in the temporal context of neuronal activity, although conventional activity-dependent LTP is seemingly absent at these synapses.

Our results further indicate that protein synthesis downstream of cholinergic stimulation and resultant CCh-LTD is required for the reinforcement of LTP at the cortical inputs to CA2 neurons. This suggests that a pool of process-independent plasticity-related proteins (PRPs) common to LTD and LTP is likely synthesized in CA2 neurons during a period of high cholinergic tone allowing for the metaplastic reinforcement of subsequently induced LTP. It is possible that the activation of M1 and M3 muscarinic AChRs, and nicotinic AChRs during CCh-LTD, plays a role in the observed metaplasticity in CA2 neurons conferred by cholinergic stimulation. Muscarinic M1 and M3 AChRs are $G_{q/11}$ -coupled receptors, downstream of which there is activation of the mitogen-activated protein kinase pathway extracellular signal-regulated kinases ERK1/2 (Lanzafame et al., 2003) known to be involved in LTP and memory (Impey et al., 1999). ERK1/2 activation has also been shown to be critical for CCh-LTD (McCoy and McMahon, 2007; Scheiderer et al., 2008). It is possible that the upregulation of such PRPs downstream of cholinergic receptor activation could potentially pivot the synapses toward persistent LTP in response to subthreshold plasticity-inducing tetanizing stimuli. mAChR activation has also been shown to be involved in mediating the learning-induced synaptic delivery of AMPARs in CA1 neurons (Mitsushima et al., 2013). CCh application has been shown in a recent study to induce CA2 pyramidal neuron depolarization and burst firing of action potentials mediated by the activation of M1 and M3 mAChRs, and not M2 mAChRs (Robert et al., 2020). The $G_{q/11}$ -mediated signal downstream of M1, M3 mAChR activation can also mobilize intracellular calcium by Ca^{2+} release from inositol 1,4,5-trisphosphate-sensitive intracellular stores, owing to phospholipase C activation (Lanzafame et al., 2003). The consequent rise in intracellular calcium levels can evoke signaling cascades that support LTP (Fernández de Sevilla et al., 2008; Karagas and Venkatachalam, 2019). Likewise, nicotinic AChRs are ligand-gated cation-permeable ion channels, some of which are permeable to calcium ions; and it is possible that a resultant increase in cytoplasmic calcium levels may ensue signal transduction cascades (Yakel, 2013) that could contribute to the observed CCh-primed LTP at CA2 synapses. Overall, it appears that a summation of multiple positive reinforcing effects in CA2 neurons downstream of activation of the cholinergic receptors implicated in CCh-LTD could serve to enhance the effectiveness of subthreshold plasticity-inducing stimuli to elicit lasting LTP, although the exact underlying mechanisms remain to be determined.

Further, while concurrent synaptic depression at SC-CA2 “cooperates” with the stable expression of CCh-primed LTP at EC-CA2, reversing the synaptic weights at SC-CA2 toward baseline “interferes” with the expression of primed LTP. This suggests a trans-compartmental regulation of synaptic weights along the proximo-distal dendritic axis of CA2 neurons such that

CCh-primed LTP at distal cortical inputs to CA2 is modulated by varying strength of concurrent synaptic responses at the proximal SC pathway. This further underscores the importance of synaptic information processing between CA3 and CA2 in the expression of synaptic plasticity and memory mediated through the stimulation of cortical inputs to CA2 neurons. This may also be regarded as a possible homeostatic mechanism to reset synaptic weights in accordance with synaptic activity patterns. Thus, metaplastic learning rules are extended to synaptic activity patterns between heterosynaptic pathways. Such metaplastic regulatory mechanisms can potentially facilitate normalization of synaptic weights (Miller, 1996; Yger and Gilson, 2015), and thereby ensure the stability of a dynamically learning neuronal network.

Collectively, the present study provides the first evidence that priming activity by cholinergic receptor activation and the resultant synaptic depression in hippocampal CA2 neurons serves as a metaplastic trigger enabling a bidirectional switch to persistent LTP at EC-CA2 and SC-CA2 synapses. Hippocampal cholinergic tone is increased during active wakefulness observed in exploration of novel environments (Giovannini et al., 2001) and during spatial learning tasks (Fadda et al., 2000). High hippocampal cholinergic tone during active wakefulness promotes theta oscillations that support memory encoding, whereas low cholinergic tone during rest promotes sharp wave-ripple oscillations that support memory consolidation (Buzsáki, 1989; Hasselmo and McGaughy, 2004; Vandecasteele et al., 2014). Thus, a dynamic modulation of CA2 cholinergic tone could potentially influence neuronal oscillations and thereby the encoding and subsequent consolidation of CA2-dependent memories. It is therefore plausible that a temporally sequenced modulation of synaptic strength at CA2 neurons subsequent to increased hippocampal cholinergic tone during exploratory behavior may contribute to the stability of encoded memories in a metaplastic manner. Given that hippocampal CA2 is implicated in spatial, social, and contextual memory (Hitti and Siegelbaum, 2014; Wintzer et al., 2014; Alexander et al., 2016), it would be of interest to study the effects of targeted activation or inactivation of basal forebrain cholinergic afferents to the CA2 area on CA2-dependent memory and behavior. These outstanding possibilities will be of interest to explore in future studies.

References

- Abraham WC (2008) Metaplasticity: tuning synapses and networks for plasticity. *Nat Rev Neurosci* 9:387.
- Abraham WC, Bear MF (1996) Metaplasticity: the plasticity of synaptic plasticity. *Trends Neurosci* 19:126–130.
- Alexander GM, Farris S, Pirone JR, Zheng C, Colgin LL, Dudek SM (2016) Social and novel contexts modify hippocampal CA2 representations of space. *Nat Commun* 7:10300.
- Bakst I, Amaral DG (1984) The distribution of acetylcholinesterase in the hippocampal formation of the monkey. *J Comp Neurol* 225:344–371.
- Benoy A, Dasgupta A, Sajikumar S (2018) Hippocampal area CA2: an emerging modulatory gateway in the hippocampal circuit. *Exp Brain Res* 236:919–931.
- Bienenstock EL, Cooper LN, Munro PW (1982) Theory for the development of neuron selectivity: orientation specificity and binocular interaction in visual cortex. *J Neurosci* 2:32–48.
- Borhegyi Z, Leranth C (1997) Substance P innervation of the rat hippocampal formation. *J Comp Neurol* 384:41–58.
- Brown DA (2019) Acetylcholine and cholinergic receptors. *Brain Neurosci Adv* 3:2398212818820506.
- Buzsáki G (1989) Two-stage model of memory trace formation: a role for 'noisy' brain states. *Neuroscience* 31:551–570.
- Carstens KE, Dudek SM (2019) Regulation of synaptic plasticity in hippocampal area CA2. *Curr Opin Neurobiol* 54:194–199.
- Carstens KE, Phillips ML, Pozzo-Miller L, Weinberg RJ, Dudek SM (2016) Perineuronal nets suppress plasticity of excitatory synapses on CA2 pyramidal neurons. *J Neurosci* 36:6312–6320.
- Chen S, He L, Huang AJ, Boehringer R, Robert V, Wintzer ME, Polygalov D, Weitemier AZ, Tao Y, Gu M, Middleton SJ, Namiki K, Hama H, Therreau L, Chevaleyre V, Hioki H, Miyawaki A, Piskorski RA, McHugh TJ (2020) A hypothalamic novelty signal modulates hippocampal memory. *Nature* 586:270–274.
- Chevaleyre V, Siegelbaum SA (2010) Strong CA2 pyramidal neuron synapses define a powerful disinaptic cortico-hippocampal loop. *Neuron* 66:560–572.
- Cui Z, Gerfen CR, Young WS 3rd (2013) Hypothalamic and other connections with dorsal CA2 area of the mouse hippocampus. *J Comp Neurol* 521:1844–1866.
- Dasgupta A, Baby N, Krishna K, Hakim M, Wong YP, Behnisch T, Soong TW, Sajikumar S (2017) Substance P induces plasticity and synaptic tagging/capture in rat hippocampal area CA2. *Proc Natl Acad Sci USA* 114:E8741–E8749.
- Dasgupta A, Lim YJ, Kumar K, Baby N, Pang KL, Benoy A, Behnisch T, Sajikumar S (2020) Group III metabotropic glutamate receptors gate long-term potentiation and synaptic tagging/capture in rat hippocampal area CA2. *Elife* 9:e55344.
- Evans PR, Parra-Bueno P, Smirnov MS, Lustberg DJ, Dudek SM, Hepler JR, Yasuda R (2018) RGS14 restricts plasticity in hippocampal CA2 by limiting postsynaptic calcium signaling. *eNeuro* 5:ENEURO0353-17.2018.
- Fadda F, Cocco S, Stancampiano R (2000) Hippocampal acetylcholine release correlates with spatial learning performance in freely moving rats. *Neuroreport* 11:2265–2269.
- Farris S, Ward JM, Carstens KE, Samadi M, Wang Y, Dudek SM (2019) Hippocampal subregions express distinct dendritic transcriptomes that reveal differences in mitochondrial function in CA2. *Cell Rep* 29:522–539.e526.
- Fernández de Sevilla D, Núñez A, Borde M, Malinow R, Buño W (2008) Cholinergic-mediated IP3-receptor activation induces long-lasting synaptic enhancement in CA1 pyramidal neurons. *J Neurosci* 28:1469–1478.
- Gaykema RP, van der Kuil J, Hersch LB, Luiten PG (1991) Patterns of direct projections from the hippocampus to the medial septum-diagonal band complex: anterograde tracing with *Phaseolus vulgaris* leucoagglutinin combined with immunohistochemistry of choline acetyltransferase. *Neuroscience* 43:349–360.
- Giovannini MG, Rakovska A, Benton RS, Pazzagli M, Bianchi L, Pepeu G (2001) Effects of novelty and habituation on acetylcholine, GABA, and glutamate release from the frontal cortex and hippocampus of freely moving rats. *Neuroscience* 106:43–53.
- Gold PE (2003) Acetylcholine modulation of neural systems involved in learning and memory. *Neurobiol Learn Mem* 80:194–210.
- Haam J, Yakel JL (2017) Cholinergic modulation of the hippocampal region and memory function. *J Neurochem* 142 Suppl 2:111–121.
- Hasselmo ME (2006) The role of acetylcholine in learning and memory. *Curr Opin Neurobiol* 16:710–715.
- Hasselmo ME, McGaughy J (2004) High acetylcholine levels set circuit dynamics for attention and encoding and low acetylcholine levels set dynamics for consolidation. *Prog Brain Res* 145:207–231.
- Hasselmo ME, Schnell E (1994) Laminar selectivity of the cholinergic suppression of synaptic transmission in rat hippocampal region CA1: computational modeling and brain slice physiology. *J Neurosci* 14:3898–3914.
- Hitti FL, Siegelbaum SA (2014) The hippocampal CA2 region is essential for social memory. *Nature* 508:88–92.
- Huber KM, Kayser MS, Bear MF (2000) Role for rapid dendritic protein synthesis in hippocampal mGluR-dependent long-term depression. *Science* 288:1254–1257.
- Huber KM, Roder JC, Bear MF (2001) Chemical induction of mGluR5- and protein synthesis-dependent long-term depression in hippocampal area CA1. *J Neurophysiol* 86:321–325.
- Ichikawa T, Hirata Y (1986) Organization of choline acetyltransferase-containing structures in the forebrain of the rat. *J Neurosci* 6:281–292.
- Impey S, Obrietan K, Storm DR (1999) Making new connections: role of ERK/MAP kinase signaling in neuronal plasticity. *Neuron* 23:11–14.
- Jedlicka P (2002) Synaptic plasticity, metaplasticity and BCM theory. *Bratislav Lek Listy* 103:137–143.

- Karagas NE, Venkatachalam K (2019) Roles for the endoplasmic reticulum in regulation of neuronal calcium homeostasis. *Cells* 8:1232.
- Kirkwood A, Rozas C, Kirkwood J, Perez F, Bear MF (1999) Modulation of long-term synaptic depression in visual cortex by acetylcholine and norepinephrine. *J Neurosci* 19:1599–1609.
- Lanzafame AA, Christopoulos A, Mitchelson F (2003) Cellular signaling mechanisms for muscarinic acetylcholine receptors. *Recept Channels* 9:241–260.
- Lee HJ, Caldwell HK, Macbeth AH, Tolu SG, Young WS (2008) A conditional knockout mouse line of the oxytocin receptor. *Endocrinology* 149:3256–3263.
- Lee SE, Simons SB, Heldt SA, Zhao M, Schroeder JP, Vellano CP, Cowan DP, Ramineni S, Yates CK, Feng Y, Smith Y, Sweatt JD, Weinshenker D, Ressler KJ, Dudek SM, Hepler JR (2010) RGS14 is a natural suppressor of both synaptic plasticity in CA2 neurons and hippocampal-based learning and memory. *Proc Natl Acad Sci USA* 107:16994–16998.
- Levey AI, Edmunds SM, Koliatsos V, Wiley RG, Heilman CJ (1995) Expression of m1-m4 muscarinic acetylcholine receptor proteins in rat hippocampus and regulation by cholinergic innervation. *J Neurosci* 15:4077–4092.
- Marder E (2012) Neuromodulation of neuronal circuits: back to the future. *Neuron* 76:1–11.
- Marino MJ, Rouse ST, Levey AI, Potter LT, Conn PJ (1998) Activation of the genetically defined m1 muscarinic receptor potentiates N-methyl-D-aspartate (NMDA) receptor currents in hippocampal pyramidal cells. *Proc Natl Acad Sci USA* 95:11465–11470.
- Massey PV, Bhabra G, Cho K, Brown MW, Bashir ZI (2001) Activation of muscarinic receptors induces protein synthesis-dependent long-lasting depression in the perirhinal cortex. *Eur J Neurosci* 14:145–152.
- McCoy PA, McMahon LL (2007) Muscarinic receptor dependent long-term depression in rat visual cortex is PKC independent but requires ERK1/2 activation and protein synthesis. *J Neurophysiol* 98:1862–1870.
- Meibach RC, Siegel A (1977) Efferent connections of the septal area in the rat: an analysis utilizing retrograde and anterograde transport methods. *Brain Res* 119:1–20.
- Mellgren SI, Harkmark W, Srebro B (1977) Some enzyme histochemical characteristics of the human hippocampus. *Cell Tissue Res* 181:459–471.
- Miller KD (1996) Synaptic economics: competition and cooperation in synaptic plasticity. *Neuron* 17:371–374.
- Mitsushima D, Sano A, Takahashi T (2013) A cholinergic trigger drives learning-induced plasticity at hippocampal synapses. *Nat Commun* 4:2760.
- Navakkode S, Sajikumar S, Frey JU (2004) The type IV-specific phosphodiesterase inhibitor rolipram and its effect on hippocampal long-term potentiation and synaptic tagging. *J Neurosci* 24:7740–7744.
- Nyakas C, Luiten PG, Spencer DG, Traber J (1987) Detailed projection patterns of septal and diagonal band efferents to the hippocampus in the rat with emphasis on innervation of CA1 and dentate gyrus. *Brain Res Bull* 18:533–545.
- Orta-Salazar E, Cuellar-Lemus CA, Díaz-Cintra S, Fera-Velasco AI (2014) Cholinergic markers in the cortex and hippocampus of some animal species and their correlation to Alzheimer's disease. *Neurologia* 29:497–503.
- Pagani JH, Zhao M, Cui Z, Avram SK, Caruana DA, Dudek SM, Young WS (2015) Role of the vasopressin 1b receptor in rodent aggressive behavior and synaptic plasticity in hippocampal area CA2. *Mol Psychiatry* 20:490–499.
- Palacios-Filardo J, Mellor JR (2019) Neuromodulation of hippocampal long-term synaptic plasticity. *Curr Opin Neurobiol* 54:37–43.
- Ransmayr G, Cervera P, Hirsch E, Ruberg M, Hersch LB, Duyckaerts C, Hauw JJ, Delumeau C, Agid Y (1989) Choline acetyltransferase-like immunoreactivity in the hippocampal formation of control subjects and patients with Alzheimer's disease. *Neuroscience* 32:701–714.
- Robert V, Therreau L, Davatolhagh MF, Bernardo-Garcia FJ, Clements KN, Chevalyere V, Piskrowski RA (2020) The mechanisms shaping CA2 pyramidal neuron action potential bursting induced by muscarinic acetylcholine receptor activation. *J Gen Physiol* 152:e201912462.
- Scheiderer CL, McCutchen E, Thacker EE, Kolasa K, Ward MK, Parsons D, Harrell LE, Dobrunz LE, McMahon LL (2006) Sympathetic sprouting drives hippocampal cholinergic reinnervation that prevents loss of a muscarinic receptor-dependent long-term depression at CA3-CA1 synapses. *J Neurosci* 26:3745–3756.
- Scheiderer CL, Smith CC, McCutchen E, McCoy PA, Thacker EE, Kolasa K, Dobrunz LE, McMahon LL (2008) Coactivation of M(1) muscarinic and alpha1 adrenergic receptors stimulates extracellular signal-regulated protein kinase and induces long-term depression at CA3-CA1 synapses in rat hippocampus. *J Neurosci* 28:5350–5358.
- Seguela P, Wadiche J, Dineley-Miller K, Dani JA, Patrick JW (1993) Molecular cloning, functional properties, and distribution of rat brain alpha 7: a nicotinic cation channel highly permeable to calcium. *J Neurosci* 13:596–604.
- Seymour-Laurent KJ, Barish ME (1995) Inositol 1,4,5-trisphosphate and ryanodine receptor distributions and patterns of acetylcholine and caffeine-induced calcium release in cultured mouse hippocampal neurons. *J Neurosci* 15:2592–2608.
- Shetty MS, Sharma M, Hui NS, Dasgupta A, Gopinadhan S, Sajikumar S (2015) Investigation of synaptic tagging/capture and cross-capture using acute hippocampal slices from rodents. *J Vis Exp* 103:e53008.
- Simons SB, Escobedo Y, Yasuda R, Dudek SM (2009) Regional differences in hippocampal calcium handling provide a cellular mechanism for limiting plasticity. *Proc Natl Acad Sci USA* 106:14080–14084.
- Sweatt JD (2010) Long-term potentiation: a candidate cellular mechanism for information storage in the central nervous system. In: *Mechanisms of memory* (Sweatt JD, ed), Ed 2, pp 150–189. London: Academic.
- Teles-Grilo Ruivo LM, Mellor JR (2013) Cholinergic modulation of hippocampal network function. *Front Synaptic Neurosci* 5:2.
- Vandecasteele M, Varga V, Berenyi A, Papp E, Bartho P, Venance L, Freund TF, Buzsáki G (2014) Optogenetic activation of septal cholinergic neurons suppresses sharp wave ripples and enhances theta oscillations in the hippocampus. *Proc Natl Acad Sci USA* 111:13535–13540.
- Volk LJ, Pfeiffer BE, Gibson JR, Huber KM (2007) Multiple Gq-coupled receptors converge on a common protein synthesis-dependent long-term depression that is affected in fragile X syndrome mental retardation. *J Neurosci* 27:11624–11634.
- Wada E, Wada K, Boulter J, Deneris E, Heinemann S, Patrick J, Swanson LW (1989) Distribution of alpha 2, alpha 3, alpha 4, and beta 2 neuronal nicotinic receptor subunit mRNAs in the central nervous system: a hybridization histochemical study in the rat. *J Comp Neurol* 284:314–335.
- Williams S, Johnston D (1990) Muscarinic depression of synaptic transmission at the hippocampal mossy fiber synapse. *J Neurophysiol* 64:1089–1097.
- Williams JH, Kauer JA (1997) Properties of carbachol-induced oscillatory activity in rat hippocampus. *J Neurophysiol* 78:2631–2640.
- Wintzer ME, Boehringer R, Polygalov D, McHugh TJ (2014) The hippocampal CA2 ensemble is sensitive to contextual change. *J Neurosci* 34:3056–3066.
- Yakel JL (2013) Cholinergic receptors: functional role of nicotinic ACh receptors in brain circuits and disease. *Pflugers Arch* 465:441–450.
- Yger P, Gilson M (2015) Models of metaplasticity: a review of concepts. *Front Comput Neurosci* 9:138.
- Yoshida K, Oka H (1995) Topographical projections from the medial septum-diagonal band complex to the hippocampus: a retrograde tracing study with multiple fluorescent dyes in rats. *Neurosci Res* 21:199–209.
- Young WS, Li J, Wersinger SR, Palkovits M (2006) The vasopressin 1b receptor is prominent in the hippocampal area CA2 where it is unaffected by restraint stress or adrenalectomy. *Neuroscience* 143:1031–1039.
- Zhao M, Choi YS, Obrietan K, Dudek SM (2007) Synaptic plasticity (and the lack thereof) in hippocampal CA2 neurons. *J Neurosci* 27:12025–12032.